

**A NON-FIBER OPTICAL SET UP  
FOR THE MEASUREMENT OF PATIENT RESPONSE TIME  
IN FUNCTIONAL MAGNETIC RESONANCE IMAGING**

By  
Mehmet ÜNSAL

Submitted to the Institute of Graduate Studies in  
Science and Engineering in partial fulfillment of  
the requirements for the degree of  
Master of Science  
in  
Electrical and Electronics Engineering

Yeditepe University  
2008

A NON-FIBER OPTICAL SET UP  
FOR THE MEASUREMENT OF PATIENT RESPONSE TIME  
IN FUNCTIONAL MAGNETIC RESONANCE IMAGING

APPROVED BY:

Assist.Prof.Dr.Ali Ümit KESKİN  
(Thesis Supervisor)

Prof.Dr. Canan Aykut BİNGÖL

Inst. Deniz PAZARCI

DATE OF APPROVAL:

## ACKNOWLEDGEMENTS

I would like to express my gratitude to the management of Yeditepe University Hospital because of their confidence and support in pursuing this project.

## **ABSTRACT**

### **A NON-FIBEROPTICAL SET UP FOR THE MEASUREMENT OF PATIENT RESPONSE TIME IN FUNCTIONAL MAGNETIC RESONANCE IMAGING**

Functional imaging is imaging which relates body function or mental activity to specific locations in the brain. It has become a powerful instrument to study local neuronal activity involved in motor, sensory and/or cognitive tasks. Extension of this technique to the spinal cord shows great promise for research and clinical applications. The current knowledge of neuroanatomy is mainly based upon invasive anatomical and pathological research. fMRI is a promising technique to demonstrate neuronal activity as it is performed in a noninvasive way. Thus the technique may have important clinical uses.

The main advantages to fMRI as a technique to image brain activity related to a specific task or sensory process include 1) the signal does not require injections of radioactive isotopes, 2) the total scan time required can be very short, i.e., on the order of 1.5 to 2.0 min per run (depending on the paradigm).

Although most fMRI examinations in routine practice employ simple patient response methods such as finger tapping, in modified fMRI examinations where the correspondence between performance and brain activation is studied, some additional instrumentation, like “patient response switch (PRS), interface and recorder” is required. PRS based instrumentation makes patient reaction times to be measured. A Fiber Optic Button Response System (FO-PRS) mainly consists of fMRI Button Response unit (e.g., Psychology Software Tools, Pittsburgh, PA) with MR Projection System. The Fiber Optic Button Response System is an fMRI ready subject response collection system which has been engineered to gather subject responses and verify signals.

The Fiber Optic Button Response Units attach to the subject's wrists and can be

adjusted during scanning. These units are completely fiber optic and connect to a fiber Optic Interface Console located in the control room through an available wave guide. The interface console provides real-time feedback of subject responses via LED indicators and includes a set of switches which can be used to make responses for the subject as needed. The system provides TTL output signals that can be used to interface with other data collection devices and software. The interface console comes with a RF Pulse that the computer interprets as another button press, allowing the user to synchronize their experiments with the MR scanner.

Such a commercially available standard unit comes with some (14-meter long) cables, and provides serial port and USB connection to the data collection computer. However, an additional waveguide is required between the patient room and the operating room. On the other hand, existing wave-guide channel may not be employed, since it may already be crowded with the earlier installed cables or the length of the supplied cables can be too short to provide the required connection. These difficulties prevent the practical use of such a technique, or require hiring of expensive skilled labor for extra cable installation, isolation and RF shielding.

At present optical means of fMRI instrumentation is preferred, because, there exist intensive electromagnetic signals generated by gradient and RF coils (during an fMRI examination, in particular). In addition, there is a strong constant magnetic field (as high as 3 Tesla) within the patient room, and optical signal processing may seem to be reasonable to avoid distortions in such an environment.

In this study, we show that relatively expensive fiber optical unit and fiber optical interface can be replaced by simple electronics without any disturbance to stimulus measuring unit as well as to the MRI. The cost of the measuring and interface unit whose performance has been reported in this work is very low as compared to commercially available equipment.

## ÖZET

# FONKSİYONEL MANYETİK REZONANS GÖRÜNTÜLEMEDE HASTA YANIT SÜRELERİNİN FİBER OPTİKSİZ ÖLÇÜMÜ İÇİN BİR SİSTEM

Fonksiyonel görüntüleme (fMRI) vücutsal işlevleri veya düşünsel aktiviteyi beyindeki belirgin bölgelerle ilintiliyen bir görüntüleme tekniğidir. Bu görüntüleme motor, duyuumsal ve/veya algılama işlemlerinde yer alan yerel nöron aktivitesinin çalışılmasında çok güçlü bir araç olmuştur. Günümüz nöroanatomi bilgisi invaziv anatomik ve patolojik araştırmalara dayanır. Öte yandan fMRI ise nöronal aktiviteyi tanımlayan invaziv olmayan bir yöntemdir. Böylelikle söz konusu teknik önemli klinik uygulamalara sahip olabilir.

Belirli bir işleve veya duyuumsal sürece bağlı beyin faaliyetlerini görüntülemeye fMRI yönteminin temel yararları şunlardır: 1- İşaret radyoaktif izotopların enjeksiyonun gerektirmez. 2-Toplam tarama süresi çok kısa olabilmektedir. (paradigmaya bağlı olarak 1.5-2 dakika mertebesindedir.)

Rutin uygulamadaki fMRI tetkiklerinin çoğunda parmak dokundurma gibi basit hasta yanıt yöntemleri kullanırken, daha gelişmiş fMRI tekniklerinde (örneğin performansla beyin aktivasyonu arasındaki ilişki çalışıldığında) bazı ilave düzenekler (örneğin hasta yanıt anahtarı, arabirim ve kayıt düzenleri) gerekir. Hasta yanıt anahtarı (PRS) hasta tepki sürelerinin ölçümünü sağlar. Bir fiberoptik anahtarlı yanıt sistemi temel olarak fMRI anahtar yanıt birimi ve MR projeksiyon sisteminden oluşur. Fiberoptik yanıt düzeni (FO-PRS) sistemi hazır denek yanıt toplama sistemidir ve deneklerden gelen yanıtları alıp işaretleri tetkik etmeye yaramaktadır.

FO-PRS'ler deneklerin (hastaların) bileklerine takılır ve tarama sırasında ayarlanabilirler. Bu birimler tamamen fiberoptiktirler ve mevcut bir dalga klavuzu aracılığıyla kontrol odasında bulunan bir fiberoptik arabirim düzenine bağlanırlar. Sistem

diğer veri toplama aygıtlarıyla ve yazılımla etkileşimde kullanılacak TTL çıkış işaretlerini üretir. Arabirim, kullanıcının deneylerini MRI cihazıyla eş güdümlü olarak kullanılmasına sağlayacak donanıma sahiptir.

Halen ticari olarak mevcut olan cihazlar veri toplama bilgisayarına USB bağlantısı ile seri terminal çıkışlarını sağlarlar, ancak hasta odasıyla kumanda odası arasında ilave bir dalga klavuzu gereklidir. Diğer yandan mevcut dalga klavuz kanalı, daha önceden montajı yapılan MRI sistemine ait kabloların sıkışıklığı nedeni ile yada gerekli bağlantının sağlanmasındaki kablo uzunluklarının yetersizliğinden dolayı kullanılamayabilir. Bu zorluklar optik tekniklerin pratik kullanımını engeller yada (ekstra kablo montajı, izolasyonu ve RF ekranlaması için) pahalı malzeme ve iş gücü kullanımını gerektirir.

Optik yöntemler (özellikle fMRI tetkikinde) gradyan ve RF bobinlerinden kaynaklanan yüksek güçlü elektromanyetik işaretlerin etkisini yok etmek amacıyla tercih edilmektedir. Bunlara ilaveten (3 Tesla gibi) yüksek bir sabit manyetik alan hasta odasında mevcut bulunmaktadır.

Bu çalışmada amaç, nispeten pahalı fiberoptik düzen ve fiberoptik arabirimin işlevinin benzerinin (uyarı ölçme düzeni ve MRI'ya etkisi olmayan) basit bir elektronik düzenle gerçekleştirilebileceği göstermektedir. Bu ölçme ve arabirim düzenin maliyeti mevcut ekipmana göre çok daha düşüktür. Çalışmada kullanılan teknik detaylı olarak açıklanarak, bir 3 Tesla MRI cihazında uygulaması ve performans sonuçları verilmiştir.

## TABLE OF CONTENTS

ACKNOWLEDGEMENTS .....	iii
ABSTRACT.....	iv
ÖZET .....	vi
LIST OF FIGURES .....	x
LIST OF TABLES.....	xii
LIST OF SYMBOLS / ABBREVIATIONS.....	xiii
1. INTRODUCTION .....	1
1.1. Overview of the Thesis .....	3
2. MRI SYSTEM PRINCIPLES .....	4
2.1. Physics of MRI.....	4
2.1.1. Precession and Larmor Frequency: .....	5
2.1.2. Pulsed Magnetic Fields.....	6
2.1.3. Spin Relaxation .....	8
2.1.4. The Time Domain NMR Signal .....	8
2.1.5. The 90-FID Sequence.....	8
2.1.5.1. The Spin-Echo Sequence.....	9
2.1.5.2. The Inversion Recovery Sequence .....	10
2.1.6. Chemical Shift.....	10
2.2. MR Imaging .....	11
2.2.1. Frequency Encoding .....	12
2.2.2. Phase Encoding Gradient .....	12
2.3. FT Tomographic Imaging .....	14
2.4. Echo planar imaging (EPI).....	17
3. FUNCTIONAL MAGNETIC RESONANCE IMAGING (fMRI) .....	21
3.1. Measuring Hemodynamic Responses .....	22
3.2. Standard Preprocessing of Images .....	25
3.3. Standard Analysis of fMRI Sequences .....	26
3.4. Combined EEG-fMRI Analysis .....	27
4. A NON-FIBER OPTICAL SET UP FOR THE MEASUREMENT OF PATIENT RESPONSE TIME IN fMRI.....	30



4.1. Materials and Methods .....	32
4.1.1. Circuit .....	34
4.2. Mutual Interaction Tests: .....	38
4.3. Additional remarks .....	39
5. CONCLUSION .....	45
REFERENCES .....	46
APPENDIX A: BS 107 TRANSISTOR DATA SHEET .....	49
APPENDIX B: BD 135 TRANSISTOR DATA SHEET .....	55

## LIST OF FIGURES

Figure 2.1. Equilibrium Magnetization.....	4
Figure 2.2. Current Direction.....	7
Figure 2.3. The relative positions of the two radio frequency pulses and SE signal .....	9
Figure 2.4. Timing diagram showing the relative positions of the two radio frequency pulses and the IR signal .....	10
Figure 2.5. Chemical Shift.....	11
Figure 2.6. MRI principle .....	11
Figure 2.7. Describing the phase encoding.....	13
Figure 2.8. The simplest FT imaging sequence.....	15
Figure 2.9. Slice selection.....	15
Figure 2.10. Picture of spins.....	16
Figure 2.11. EPI sequence .....	18
Figure 2.12. Expanded EPI sequence .....	19
Figure 3.1. An example of HRF projected using Benar method, from a time scale of -18 seconds prior to the event to 48 seconds after the event .....	24
Figure 3.2. Examples of BOLD signal .....	28

Figure 3.3. A statistical map of activation in a patient with left temporal spikes. Note the main area of activation on the left side, and the small activation in the contra-lateral area on the right .....	29
Figure 4.1. Block diagram of the patient response measuring system .....	33
Figure 4.2.1. Transmitter cone.....	34
Figure 4.2.2. Transmitter cone, front view .....	36
Figure 4.3. Image projector, the receiver sensor and electronics (upper right) in the operating room.....	36
Figure 4.4. Semi-transparent image display screen .....	37
Figure 4.5. The patient response circuit.....	37
Figure 4.6. Computer interface circuit using DAQ card (National Instruments, DAQmx) .....	38
Figure 4.7. Transmitter side, voltage pulses at the gate of the MOSFET (upper trace, CH1) and the base of BJT (CH2).....	40
Figure 4.8. Transmitter side expanded time scale view of voltage pulses at the gate of the MOSFET (upper trace, CH1) and the base of BJT (CH2) .....	40
Figure 4.9. Transmitter side voltage pulses at the gate of the MOSFET (CH1) and the collector of BJT (CH2). This record demonstrates the time delay caused by incandescent mini-lamp .....	41
Figure 4.10. The overall response.....	41
Figure 4.11. Time expanded view of Overall response.....	42

**LIST OF TABLES**

Table 4.1. Reaction Time of Patients.....42

**LIST OF SYMBOLS / ABBREVIATIONS**

ADC	Analog to Digital Converter
BOLD	Blood Oxygen Level Dependent
CNR	Contrast to noise ratio
CSF	Cerebrospinal fluid
DAC	Digital to Analog Converter
DAQ	Data Acquisition Card
EEG	Electro Encephalograph
EPI	Echoplanar Imaging
EMI	Elektromagnetic Interference
FID	Free Induction Decay
FT	Fourier Transform
fMRI	Functional MR Imaging
HRF	Hemodynamic Response Function
ICA	Independent Component Analysis
MR	Magnetic Resonance
NMR	Nuclear Magnetic Resonance
PC	Personal Computer
PET	Positron Emission Tomography
PCB	Printed Circuit Board
ROI	Region of Interest
SPM	Statistical Parametric Map
TE	Echo time
TR	Pulse repetition period

## 1. INTRODUCTION

Fundamentally, all MR-imaging is based on the interaction between the imaged tissue, externally applied magnetic fields and carefully synchronized radio frequency pulses.

Protons have a magnetic property called *spin*, which behave like an ordinary dipole-magnet. Usually, the focus of interest is on hydrogen nuclei, because of their abundance in all tissue types and relatively simple spin behavior. (The behavior of the nuclear spin of heavier atoms is more complicated, since there are internal interactions between the individual particles). Under a strong and uniform magnetic field, the spins try to align parallel to the field either in the same or opposite directions. The spins precess around those directions in a minimum energy state. Although the precession is not coherent, all the spins have a characteristic resonance frequency, proportional to the strength of the magnetic field. When a radio pulse in the resonance frequency is emitted, the spins absorb the energy and are forced into coherent precession. After the pulse, the absorbed energy decays in a relaxation process. The process is actually quite complex, for example, due to possible internal interactions in the tissue. However, signals measuring the decay of energy make the imaging possible, and adjusting the properties and timing of the radio pulses produces signals related to different aspects of the relaxation process.

To produce a volumetric (3-dimensional) image, the behavior of the spins is controlled more precisely with two gradient magnetic fields, which are perpendicular to each other. The first is applied in the same direction as the uniform magnetic field, causing the total strength of the field to change slightly along that direction. This makes the resonance frequency of the spins also different along its axis. The other gradient field is similar, but turned on and off repeatedly. As the spins precess faster during the application of the field, the spins along its axis accumulate different phases. The gradient magnetic fields allow focusing on a planar slice, which is defined by the axes of frequency-phase space. Carefully synchronizing the radio pulses with the fields produces signals originating from different parts of the slice. Additionally, the thickness of the slice can be controlled with the bandwidth of the radio pulses.

Using standard signal processing techniques, the measurements can be turned into an image of the focused slice. The full volume is produced by scanning several adjacent slices, one after the other. The image *voxels* contain a kind of density measure based on the scanning parameters and the properties of the tissue. For example, with certain parameters the image is directly related to the proton density of the tissue.

The scanning is actually very slow since the relaxation process, and adjusting the magnetic fields, requires a certain amount of time. Producing high resolution images can take several minutes. Naturally, the quality of the images is strongly affected by inhomogeneities in the magnetic fields, the internal magnetic interactions and electromagnetic interference from the environment.

Since MRI is virtually noninvasive and is able to produce high quality images, it has quickly become very popular in structural imaging. These properties are crucial also in functional imaging, but the measures used in structural MRI, such as the proton density, are not directly related to neuronal activation. Coincidentally, the scanning parameters can be tuned so that the resulting images provide a measure related to the oxygenation level in the tissue. The measure is based on the differing magnetic properties of oxygenated and deoxygenated hemoglobin molecules. The idea in functional MRI is to record a sequence of such images at different time points to allow the local changes in oxygenation level to be analyzed.

Problems arise from the long duration of the scanning. Scanning intervals of several minutes would not allow accurate analysis of the activity in the brain. Additionally, movement of the head and other physiological changes during the long exposures would distort the images. Fortunately, the scanning parameters, mainly the timing of the radio pulses, can be adjusted to allow much faster scanning. However, the spatial resolution suffers greatly from such adjustments. For example, the relaxation process is not allowed to fully complete, resulting in much weaker signals. Therefore, the setup used in fMRI is a careful compromise between fast scanning and high resolution images. Current fMRI scanners are able to produce full head volumes with a time interval of a few seconds, but the spatial resolution is only a fraction of that used in structural imaging.

## **1.1. Overview of the Thesis**

This thesis consists of three main chapters and a conclusion. The physics principles and properties of an MRI system, its components and scan sequences are explained in Chapter 2. Properties of functional MRI techniques and its working principles are explained in Chapter 3. Designed electronic control system components are explained in Chapter 4. Then, thesis is ends with the conclusion section.





## 2. MRI SYSTEM PRINCIPLES

### 2.1. Physics of MRI

When placed in a magnetic field of strength  $B$ , a particle with a net spin can absorb a photon, of frequency  $\nu$ . [1] The frequency  $\nu$  depends on the gyromagnetic ratio,  $\gamma$  of the particle, as  $\nu = \gamma B$ . For hydrogen,  $\gamma = 42.58 \text{ MHz / T}$ . Therefore, in a 3 Tesla magnet,

$$\nu = 3 \times 42.58 = 127.74 \text{ MHz} \quad (2.1)$$

When the proton is placed in an external magnetic field, the spin vector of the particle aligns itself with the external field, just like a magnet would. There is a low energy configuration or state where the poles are aligned N-S-N-S and a high energy state N-N-S-S. At equilibrium, the net magnetization vector lies along the direction of the applied magnetic field  $B_0$  and is called the equilibrium magnetization  $M_0$ . In this configuration, the Z component of magnetization  $M_Z$  equals  $M_0$ .  $M_Z$  is referred to as the longitudinal magnetization. There is no transverse ( $M_X$  or  $M_Y$ ) magnetization here, as shown in Fig.2.1.

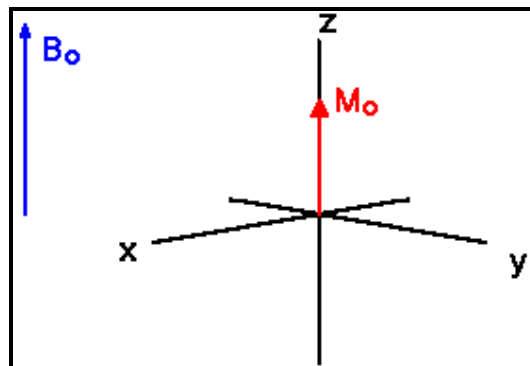


Figure 2.1. Equilibrium Magnetization

It is possible to change the net magnetization by exposing the nuclear spin system to energy of a frequency equal to the energy difference between the spin states. If enough energy is put into the system, it is possible to saturate the spin system and make  $M_Z = 0$ .

The equation governing this behavior as a function of the time  $t$  after its displacement is:

$$M_z = M_0 ( 1 - e^{-t/T_1} ) \quad (2.2)$$

$T_1$  is the time to reduce the difference between the longitudinal magnetization ( $M_z$ ) and its equilibrium value by a factor of  $e$ .

If the net magnetization is placed along the  $-Z$  axis, it will gradually return to its equilibrium position along the  $+Z$  axis at a rate governed by  $T_1$ . The equation governing this behavior as a function of the time  $t$  after its displacement is:

$$M_z = M_0 ( 1 - 2e^{-t/T_1} ) \quad (2.3)$$

Again, the spin-lattice relaxation time ( $T_1$ ) is the time to reduce the difference between the longitudinal magnetization ( $M_z$ ) and its equilibrium value by a factor of  $e$ .

### 2.1.1. Precession and Larmor Frequency:

If the net magnetization is placed in the  $XY$  plane it will rotate about the  $Z$  axis at a frequency equal to the frequency of the photon which would cause a transition between the two energy levels of the spin. This frequency is called the Larmor frequency.

In addition to the rotation, the net magnetization starts to dephase because each of the spin packets making it up is experiencing a slightly different magnetic field and rotates at its own Larmor frequency. Here the net magnetization vector is initially along  $+Y$ . For this and all dephasing examples think of this vector as the overlap of several thinner vectors from the individual spin packets.

The time constant which describes the return to equilibrium of the transverse magnetization,  $M_{XY}$ , is called the spin-spin relaxation time,  $T_2$ .

$$M_{XY} = M_{XY0} e^{-t/T_2} \quad (2.4)$$

$T_2$  is always less than or equal to  $T_1$ . The net magnetization in the XY plane goes to zero and then the longitudinal magnetization grows in until we have  $M_0$  along Z.

In summary, the spin-spin relaxation time,  $T_2$ , is the time to reduce the transverse magnetization by a factor of e. In the previous sequence,  $T_2$  and  $T_1$  processes are shown separately for clarity. That is, the magnetization vectors are shown filling the XY plane completely before growing back up along the Z axis. Actually, both processes occur simultaneously with the only restriction being that  $T_2$  is less than or equal to  $T_1$ .

Two factors contribute to the decay of transverse magnetization.

- Molecular interactions (said to lead to a *pure*  $T_2$  molecular effect)
- Variations in  $B_0$  (said to lead to an *inhomogeneous*  $T_2$  effect)

The combination of these two factors is what actually results in the decay of transverse magnetization. The combined time constant is called  $T_2$  star and is given the symbol  $T_2^*$ . The relationship between the  $T_2$  from molecular processes and that from inhomogeneities in the magnetic field is as follows.

$$1/T_2^* = 1/T_2 + 1/T_{2\text{inhomo}}. \quad (2.4)$$

### 2.1.2. Pulsed Magnetic Fields

A coil of wire placed around the X axis will provide a magnetic field along the X axis when a direct current is passed through the coil. An alternating current will produce a magnetic field which alternates in direction, Fig.2.2.

This is the same as moving the coil about the rotating frame coordinate system at the Larmor Frequency. In magnetic resonance, the magnetic field created by the coil passing an alternating current at the Larmor frequency is called the  $B_1$  magnetic field. When the alternating current through the coil is turned on and off, it creates a pulsed  $B_1$  magnetic field along the X' axis.

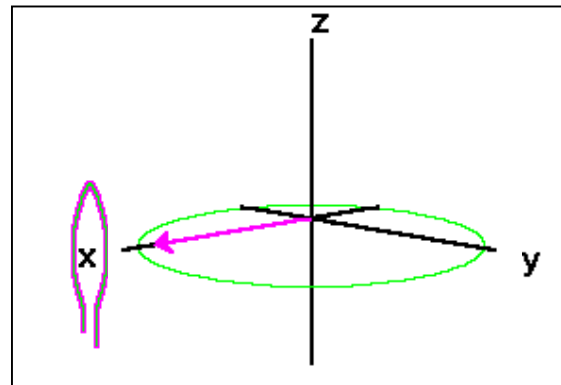


Figure 2.2. Current Direction

The spins respond to this pulse in such a way as to cause the net magnetization vector to rotate about the direction of the applied  $B_1$  field. The rotation angle depends on the length of time the field is on,  $\tau$  and its magnitude  $B_1$ .

$$\theta = 2\pi \gamma \tau B_1. \quad (2.5)$$

In our examples,  $\tau$  will be assumed to be much smaller than  $T_1$  and  $T_2$ .

A  $90^\circ$  pulse is one which rotates the magnetization vector clockwise by 90 degrees about the  $X'$  axis. A  $90^\circ$  pulse rotates the equilibrium magnetization down to the  $Y'$  axis. In the laboratory frame the equilibrium magnetization spirals down around the  $Z$  axis to the  $XY$  plane.

An  $180^\circ$  pulse will rotate the magnetization vector by 180 degrees. A  $180^\circ$  pulse rotates the equilibrium magnetization down to along the  $-Z$  axis.

The net magnetization at any orientation will behave according to the rotation equation. For example, a net magnetization vector along the  $Y'$  axis will end up along the  $-Y'$  axis when acted upon by an  $180^\circ$  pulse of  $B_1$  along the  $X'$  axis.

A net magnetization vector between  $X'$  and  $Y'$  will end up between  $X'$  and  $-Y'$  after the application of a  $180^\circ$  pulse of  $B_1$  applied along the  $X'$  axis.

### 2.1.3. Spin Relaxation

Motions in solution which result in time varying magnetic fields cause spin relaxation.

Time varying fields at the Larmor frequency cause transitions between the spin states and hence a change in  $M_z$ . There is a distribution of rotation frequencies in a sample of molecules. Only frequencies at the Larmor frequency affect  $T_1$ . Since the Larmor frequency is proportional to  $B_0$ ,  $T_1$  will therefore vary as a function of magnetic field strength. In general,  $T_1$  is inversely proportional to the density of molecular motions at the Larmor frequency.

The temperature of the human body does not vary by enough to cause a significant influence on  $T_1$ . The viscosity does however vary significantly from tissue to tissue and influences  $T_1$ .

### 2.1.4. The Time Domain NMR Signal

As transverse magnetization rotates about the Z axis, it will induce a current in a coil of wire located around the X axis. Plotting current as a function of time gives a sine wave. This wave will of course decay with time constant  $T_2^*$  due to dephasing of the spin packets. This signal is called free induction decay (FID). The FID is converted into a frequency domain spectrum.

### 2.1.5. The 90-FID Sequence

A set of RF pulses applied to a sample to produce a specific form of NMR signal is called a pulse sequence. In the 90-FID pulse sequence, net magnetization is rotated down into the X'Y' plane with a  $90^\circ$  pulse. The net magnetization vector begins to precess about the +Z axis. The magnitude of the vector also decays with time.

A timing diagram is a multiple axis plot of some aspect of a pulse sequence versus time. A timing diagram for a 90-FID pulse sequence has a plot of RF energy versus time and another for signal versus time.

When this sequence is repeated, for example when signal-to-noise improvement is needed, the amplitude of the signal after being Fourier transformed ( $S$ ) will depend on  $T_1$  and the time between repetitions, called the repetition time ( $TR$ ), of the sequence. In the signal equation below,  $k$  is proportionality constant and  $\rho$  is the density of spins in the sample.

$$S = k \rho (1 - e^{-TR/T_1}) \quad (2.5)$$

### 2.1.5.1. The Spin-Echo Sequence

Here a  $90^\circ$  pulse is first applied to the spin system. The  $90^\circ$  degree pulse rotates the magnetization down into the  $X'Y'$  plane. The transverse magnetization begins to dephase.

At some point in time after the  $90^\circ$  pulse, a  $180^\circ$  pulse is applied. This pulse rotates the magnetization by  $180^\circ$  about the  $X'$  axis.

The  $180^\circ$  pulse causes the magnetization to at least partially rephase and to produce a signal called an echo, Fig.2.3.

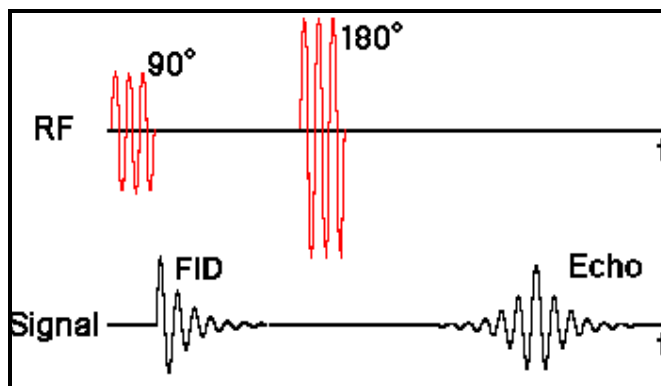


Figure 2.3. The relative positions of the two radio frequency pulses and SE signal

The signal equation for a repeated spin echo sequence as a function of the repetition time, TR, and the echo time (TE) defined as the time between the 90° pulse and the maximum amplitude in the echo is

$$S = k \rho (1 - e^{-TR/T1}) e^{-TE/T2} \quad (2.6)$$

### 2.1.5.2. The Inversion Recovery Sequence

In this sequence, an 180° pulse is first applied. This rotates the net magnetization down to the -Z axis. The magnetization undergoes spin-lattice relaxation and returns toward its equilibrium position along the +Z axis. Before it reaches equilibrium, a 90° pulse is applied which rotates the longitudinal magnetization into the XY plane. Once magnetization is present in the XY plane it rotates about the Z axis and de-phases giving a FID. Once again, the timing diagram shows the relative positions of the two radio frequency pulses and the signal, Fig.2.4.

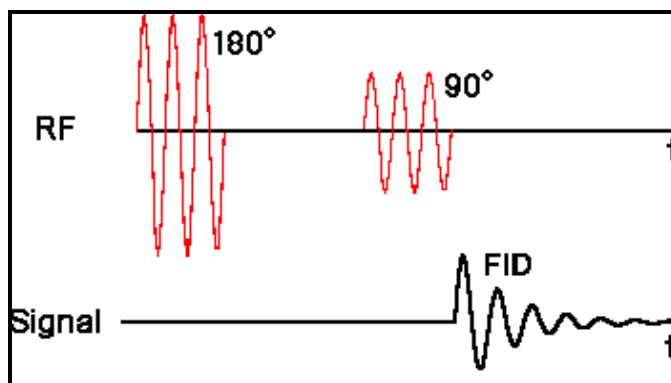


Figure 2.4. Timing diagram showing the relative positions of the two radio frequency pulses and the IR signal

### 2.1.6. Chemical Shift

When an atom is placed in a magnetic field, its electrons circulate about the direction of the applied magnetic field. This circulation causes a small magnetic field at the nucleus which opposes the externally applied field, Fig.2.5.

The magnetic field at the nucleus (the effective field) is therefore generally less than the applied field. The electron density around each nucleus in a molecule varies according to the types of nuclei and bonds in the molecule. The opposing field and therefore the effective field at each nucleus will vary. This is called the chemical shift phenomenon.

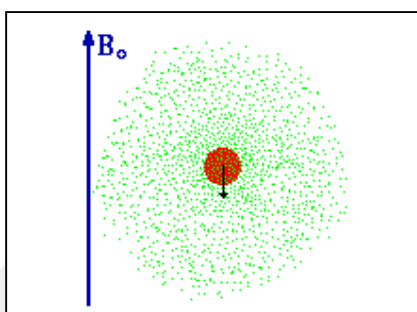


Figure 2.5. Chemical Shift

## 2.2. MR Imaging

Assume that a human head contains only three small distinct regions where there is hydrogen spin density. In reality the entire head would contain signal. When these regions of spin are experiencing the same general magnetic field strength, there is only one peak in the NMR spectrum.

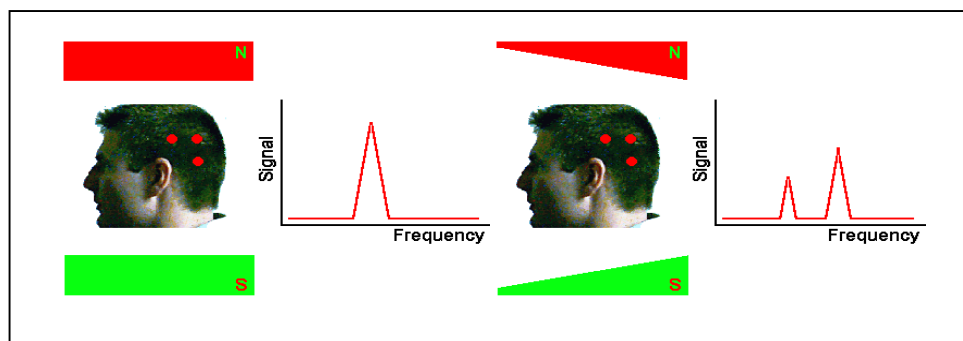


Figure 2.6. MRI principle

A gradient in the magnetic field allows to accomplish a unique magnetic field to image spin positions. A magnetic field gradient is a variation in the magnetic field with respect to position. A one-dimensional magnetic field gradient is a variation with respect to



one direction, while a two-dimensional gradient is a variation with respect to two. The most useful type of gradient in magnetic resonance imaging is a one-dimensional linear magnetic field gradient. A one-dimensional magnetic field gradient along the x axis in a magnetic field,  $B_0$ , indicates that the magnetic field is increasing in the x direction. Here the length of the vectors represent the magnitude of the magnetic field. The symbols for a magnetic field gradient in the x, y, and z directions are  $G_x$ ,  $G_y$ , and  $G_z$ .

### 2.2.1. Frequency Encoding

The point in the center of the magnet where  $(x,y,z) = 0,0,0$  is called the isocenter of the magnet. The magnetic field at the isocenter is  $B_0$  and the resonant frequency is  $\nu_0$ . If a linear magnetic field gradient is applied to our hypothetical head with three spin containing regions, the three regions experience different magnetic fields.

The result is an NMR spectrum with more than one signal. The amplitude of the signal is proportional to the number of spins in a plane perpendicular to the gradient. This procedure is called frequency encoding and causes the resonance frequency to be proportional to the position of the spin.

$$\nu = \gamma ( B_0 + x G_x ) = \nu_0 + \gamma x G_x \quad (2.7)$$

$$x = ( \nu - \nu_0 ) / ( \gamma G_x ) \quad (2.8)$$

This principle forms the basis behind all magnetic resonance imaging, Fig.2.6.

### 2.2.2. Phase Encoding Gradient

The phase encoding gradient is a gradient in the magnetic field  $B_0$ . The phase encoding gradient is used to impart a specific phase angle to a transverse magnetization vector. The specific phase angle depends on the location of the transverse magnetization vector. For example, lets imagine we have three regions with spin. The transverse magnetization vector from each spin has been rotated to a position along the X axis.

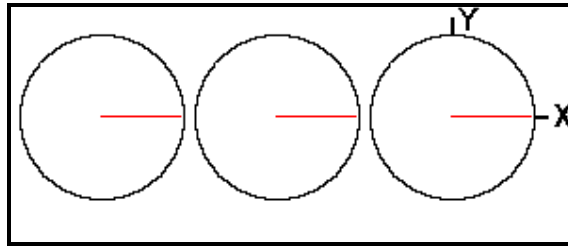


Figure 2.7. Describing the phase encoding

The three vectors have the same chemical shift and hence in a uniform magnetic field they will possess the same Larmor frequency, Fig.2.7.

If a gradient in the magnetic field is applied along the X direction the three vectors will precess about the direction of the applied magnetic field at a frequency given by the resonance equation.

$$\nu = \gamma ( B_0 + x G_x ) = \nu_0 + \gamma x G_x \quad (2.9)$$

While the phase encoding gradient is on, each transverse magnetization vector has its own unique Larmor frequency. Thus far, the description of phase encoding is the same as frequency encoding. Now for the difference. If the gradient in the X direction is turned off, the external magnetic field experienced by each spin vector is, for all practical purposes, identical. Therefore the Larmor frequency of each transverse magnetization vector is identical.

The phase angle,  $\phi$ , of each vector, on the other hand, is not identical. The phase angle being the angle between a reference axis, say the Y axis, and the magnetization vector at the time the phase encoding gradient has been turned off. There are three distinct phase angles in this example.

Just as in the examples of the frequency encoding gradient, if we had some way of measuring the frequency (in this case phase) of the spin vectors we could assign them a position along the X axis.

### 2.3. FT Tomographic Imaging

One of the best ways to understand a new imaging sequence is to examine a timing diagram for the sequence. The timing diagram for an imaging sequence has entries for the radio frequency, magnetic field gradients, and signal as a function of time. The simplest FT imaging sequence contains a  $90^\circ$  slice selective pulse, a slice selection gradient pulse, a phase encoding gradient pulse, a frequency encoding gradient pulse, and a signal. Fig.2.8

The pulses for the three gradients represent the magnitude and duration of the magnetic field gradients. The first event to occur in this imaging sequence is to turn on the slice selection gradient. The slice selection RF pulse is applied at the same time. The slice selective RF pulse is an apodized sinc function shaped burst of RF energy. Once the RF pulse is complete the slice selection gradient is turned off and a phase encoding gradient is turned on. Once the phase encoding gradient has been turned off a frequency encoding gradient is turned on and a signal is recorded. The signal is in the form of a free induction decay. This sequence of pulses is usually repeated 128 or 256 times to collect all the data needed to produce an image. The time between the repetitions of the sequence is called the repetition time, TR. Each time the sequence is repeated the magnitude of the phase encoding gradient is changed. The magnitude is changed in equal steps between the maximum amplitude of the gradient and the minimum value.

The slice selection gradient is always applied perpendicular to the slice plane. The phase encoding gradient is applied along one of the sides of the image plane. The frequency encoding gradient is applied along the remaining edge of the image plane. Imagine a cube of spins placed in a magnetic field, Fig.2.9.

The cube is composed of several volume elements each with its own net magnetization vector. Suppose we wish to image a slice in the XY plane. The  $B_0$  magnetic field is along the Z axis. The Slice selection gradient is applied along the Z axis. The RF pulse rotates only those spins packets within the cube which satisfy the resonance condition. These spin packets are located within an XY plane in this example. The location of the plane along the Z axis with respect to the isocenter is given by  $Z = \Delta\nu / \gamma G_s$  where

$\Delta v$  is the frequency offset from  $\nu_0$  ( *i.e.*  $\nu - \nu_0$  ),  $G_s$  the magnitude of the slice selection gradient, and  $\gamma$  the gyromagnetic ratio. Spins located above and below this plane are not affected by the RF pulse. To simplify the remainder of the presentation, concentrate on a  $3 \times 3$  subset of the net magnetization vectors. The picture of these spins in this plane looks like as in Fig.2.10.

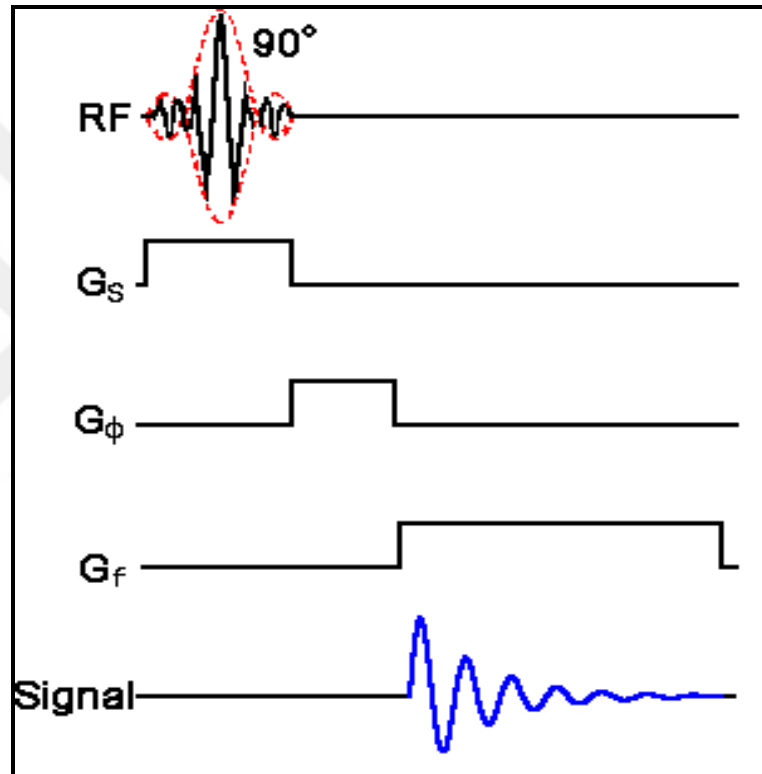


Figure 2.8. The simplest FT imaging sequence

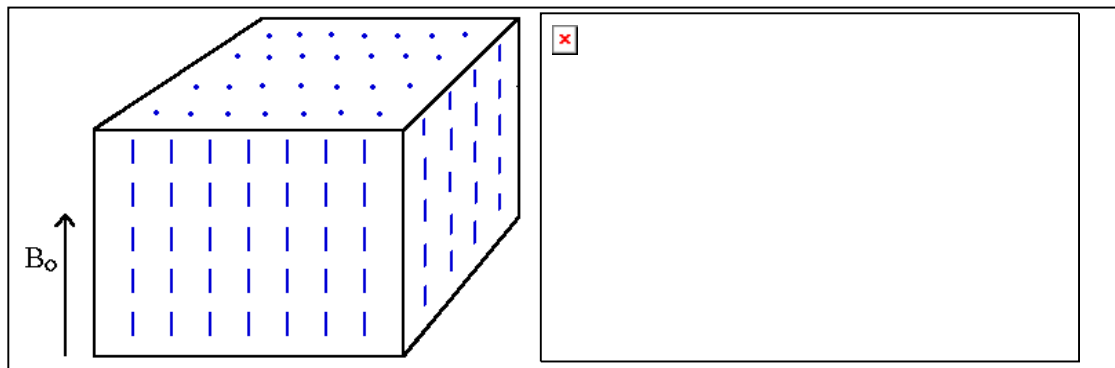


Figure 2.9. Slice selection

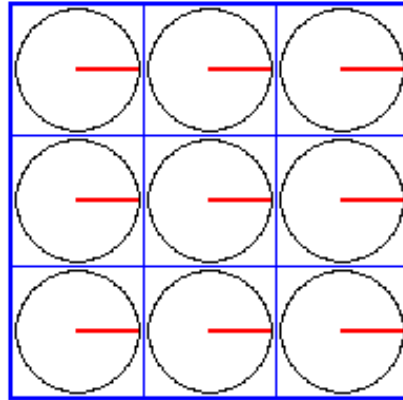


Figure 2.10. Picture of spins

Once rotated into the  $XY$  plane these vectors would precess at the Larmor frequency given by the magnetic field each was experiencing. If the magnetic field was uniform, each of the nine precessional rates would be equal. In the imaging sequence a phase encoding gradient is applied after the slice selection gradient. Assuming this is applied along the  $X$  axis, the spins at different locations along the  $X$  axis begin to precess at different Larmor frequencies. When the phase encoding gradient is turned off the net magnetization vectors precess at the same rate, but possess different phases. The phase being determined by the duration and magnitude of the phase encoding gradient pulse.

Once the phase encoding gradient pulse is turned off a frequency encoding gradient pulse is turned on. In this example the frequency encoding gradient is in the  $-Y$  direction. The frequency encoding gradient causes spin packets to precess at rates dependent on their  $Y$  location. Please note that now each of the nine net magnetization vectors is characterized by a unique phase angle and precessional frequency. If we had a means of determining the phase and frequency of the signal from a net magnetization vector we could position it within one of the nine elements.

A simple Fourier transform is capable of this task for a single net magnetization vector located somewhere within the  $3 \times 3$  space. For example, if a single vector was located at  $(X, Y) = 2, 2$ , its FID would contain a sine wave of frequency 2 and phase 2. A Fourier transform of this signal would yield one peak at frequency 2 and phase 2. Unfortunately a one dimensional Fourier transform is incapable of this task when more than one vector is

located within the  $3 \times 3$  matrix at a different phase encoding direction location. There needs to be one phase encoding gradient step for each location in the phase encoding gradient direction. The point is you need one equation for each unknown you are trying to solve for. Therefore if there are three phase encoding direction locations we will need three unique phase encoding gradient amplitudes and have three unique free induction decays. If we wish to resolve 256 locations in the phase encoding direction we will need 256 different magnitudes of the phase encoding gradient and will record 256 different free induction decays.

#### **2.4. Echo planar imaging (EPI)**

Echo planar imaging is a rapid MRI technique which is capable of producing tomographic images at video rates. The technique records an entire image in a TR period.

While MRI as conventionally practiced builds up the data for an image from a series of discrete signal samples, EPI is a method to form a complete image from a single data sample, or a single "shot". A typical T2-weighted imaging series requires that the time between excitation pulses, known as "TR" be two to three times longer than the intrinsic tissue magnetization parameter, T1. The T1 of biological samples is typically on the order of a second or so (cerebrospinal fluid, or CSF, can have much longer T1's of several seconds); TR must therefore be 3 seconds or more. A typical MR image is formed from 128 repeated samples, so that the imaging time for T2 weighted scan is about 384 seconds or more than 6.5 minutes. By comparison, the EPI approach collects all of the image data, for an image of the same resolution, in 40 to 150 milliseconds (depending on hardware and contrast considerations). This reflects a nearly 10,000-fold speed gain.

Although, there are myriad variations, EPI is fundamentally just a trick of spatial encoding. To understand the difference between EPI and conventional imaging, it is necessary therefore, to have some understanding of spatial encoding in MRI.

A magnetic resonance image is referred to as image space, while its Fourier transform is referred to as being k-space. The k-space is equivalent to the space defined by the frequency and phase encoding directions. Conventional imaging sequences record one

line of k-space each phase encoding step. Since one phase encoding step occurs each TR seconds the time required to produce an image is determined by the product of TR and the number of phase encoding steps. On the other hand, Echo planar imaging measures all lines of k-space in a single TR period.

A timing diagram for an echo planar imaging sequence looks as in Fig. 2.11 The three axes used for spatial encoding of MR images. One dimension of spatial encoding is achieved by slice selective excitation (the "Slice Selection" axis). The other two are encoded by phase and frequency. (Some texts refer to the Slice Selection axis as the "Z" axis. The Readout axis is variously labeled the "Frequency" or "X" axis; the Phase Encoding axis is sometimes labeled the "Y" axis.)

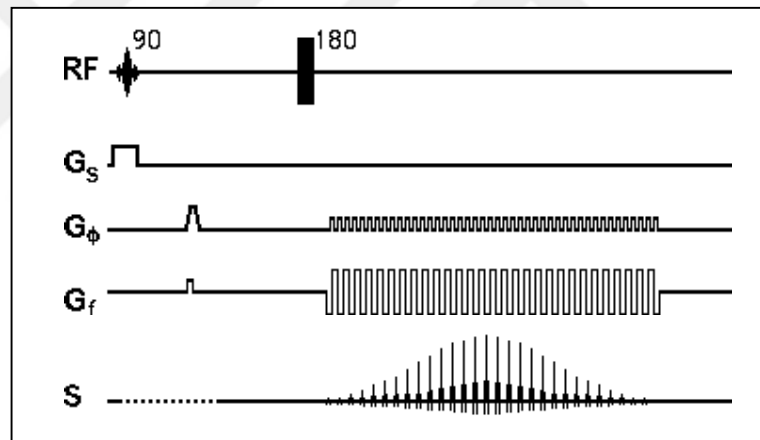


Figure 2.11. EPI sequence

There is a  $90^\circ$  slice selective RF pulse which is applied in conjunction with a slice selection gradient  $G_s$ . There is an initial phase encoding gradient pulse  $G(\phi)$  to position the spins at the corner of k-space. Next there is an  $180^\circ$  RF pulse. Since the echo planar sequence is typically a single slice sequence, the  $180^\circ$  pulse need not be a slice selective pulse. The phase and frequency encoding directions are next cycled so as to traverse k-space. This is equivalent to putting 128 or 256 phase and frequency encoding gradients in the usual period when the echo is recorded. If we zoom into this region of the timing diagram it will be clearer. One can see that in Fig 2.12 there is a phase encoding gradient, followed by a frequency encoding gradient, during which time a signal is recorded. Next there is another phase encoding

gradient followed by the reverse polarity frequency encoding gradient during which time a signal is recorded.

Looking at the k-space trajectory map at the same time as we are zoomed into the phase and frequency encoding gradient area one can see how the gradients trace out k-space. The rate at which k-space is traversed is so rapid that it is possible, depending on the image matrix, to obtain 15 to 30 images a second. This is video rate acquisition.

The imaging speed in EPI comes from the use of very high amplitude field gradients which, in turn allow, and require, very rapid sampling. While conventional MR imaging may use receiver bandwidths up to about 32 kHz, bandwidths of 300 kHz are typical in EPI and drop the usable SNR by about two-thirds. (Field strength, and RF coil considerations are not pulse-sequence dependent.)

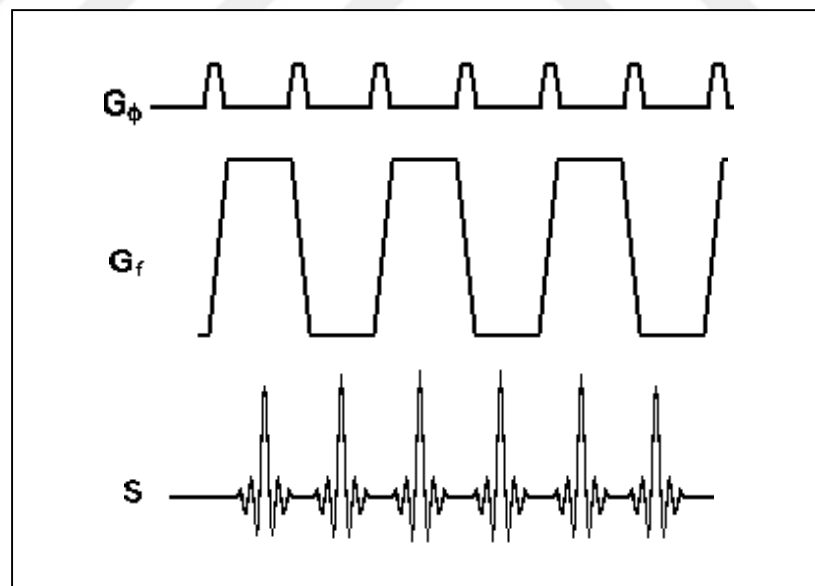


Figure 2.12. Expanded EPI sequence

In conclusion, Echo-planar imaging is the fastest approach to MR imaging, offering considerable freedom in the selection of contrast and resolution parameters. It is, however, a technologically challenging method that requires that the imaging system operate at near its performance limits in gradient amplitude and rise times, system stability, and overall



noise figure. Further, EPI can suffer from serious artifacts in shape distortion and image ghosts that require extra attention from the researcher. All told, however, the decided advantages of EPI in functional neuroimaging have placed it very much in demand for fMRI applications and have served to drive the technology development both in the academic research laboratory and with major commercial vendors.



### 3. FUNCTIONAL MAGNETIC RESONANCE IMAGING (fMRI)

Functional magnetic resonance imaging (fMRI) can be defined as a noninvasive technique used to detect brain activity. It utilizes the fact that the MR signal intensity is correlated with the cerebral blood flow, which in turn is correlated with neural activity. Most of the data analysis approaches used in fMRI have their origin in the methodology of positron emission tomography (PET) activation imaging. Both PET and fMRI take advantage of local changes in blood flow associated with increased or decreased neural activity. With PET, local increases in bloodflow result in accumulation of radioactive tracer - typically collected over 30 s or so - the image intensity reflects the integral of the underlying neural activity. In fMRI, the images are acquired much more rapidly [using echo-planar imaging acquisition times of less than 0.1 s are common] and the time course of the blood flow changes is revealed. The observed signal intensity change in MRI lags the stimulus by several seconds. Blood flow changes display a multiphasic time course, presumably reflecting an initial oxygen depletion of the capillary bed, with a response latency of about 2 s, followed by a hyperoxygenation condition, in which increased blood flow exceeds local metabolic demand. In addition to displaying a complex time course, the magnitude of the fMRI response does not bear an obvious simple relationship to either the underlying neural activity or the behavior. MR signal intensities are traditionally expressed in arbitrary units, because many factors affect the absolute signal intensity—tissue conductivity, coil placement, pulse sequence timing, tissue orientation, and magnetic field strength all play major roles. A consequence is that there exists no standard metric by which to describe the fMRI signal changes, making comparisons across studies difficult.

The signal changes typically occur in a background of substantial signal fluctuation that is not well correlated with the stimuli contrast to noise ratios (CNRs) of 3 or 4 to 1 are typical, and a CNR of more than 8 is very unusual (and probably associated with large vessels). Thus, one of the key challenges in fMRI is the artifact-free detection of these small signal changes. One strategy has been to look for changes in the mean signal intensity of the MR data during different behavioral conditions using Student's  $t$  test, where no temporal information is available (as in traditional PET experiments). An alternative, though conceptually similar, analysis is to compare the intensity distributions

in the behavioral conditions using the Kolmogorov-Smirnov (K-S) statistic. The K-S test can also be used to detect other differences in distribution, such as increased variance. It is a useful test when very little *a priori* information is available to differentiate the MR signal under different conditions. Some authors have advocated the use of “split-half”  $t$  test, which requires that the same pixel location exceed some predetermined  $t$  threshold on two independent acquisitions [2]; Some have incorporated additional criteria, such as the number of contiguous locations of increased signal intensity [3], which impose somewhat arbitrary constraints on the minimum size of an “activated” brain region. An approach using multiple linear regression was recently outlined by [4] that takes into account the time course of the fMRI signal in calculating  $t$  statistics.

An alternative method, pioneered by Bandettini, is to use correlation statistics to estimate the extent to which the signal in any pixel covaries with the behavioral conditions [5].

The fMRI can localize brain regions that show significant neural activity upon stimulus presentation. The stimulus is designed to activate the sensory, motor or cognitive task under study. fMRI data sets typically consist of time series associated with the voxels of the brain. For each voxel, the significance of the response to the stimulus is assessed by statistically analyzing the associated fMRI time series. In this way, brain activation maps, or statistical parametric maps (SPMs), can be constructed. A common approach in this analysis is to apply a general linear model to the time series of fMRI data [6] [7]. It can be assumed that the fMRI time series  $x(t)$  is a convolution of the external stimulus  $s(t)$  with a certain hemodynamic response function (HRF)  $h(t)$ , corrupted by Gaussian distributed noise  $v(t)$ . Then standard statistical tools such as the Student-t test and the F test can be used to obtain SPMs.

### 3.1. Measuring Hemodynamic Responses

The detection of changes due to neuronal activation in fMRI is based on the differing magnetic properties of oxygenated (diamagnetic) and deoxygenated (paramagnetic) hemoglobin molecules. Neuronal activation results in a localized change of blood flow and oxygenation levels, which can be measured using suitable scanning parameters. This

produces a measure called blood oxygenation level dependent (BOLD) signal. These vascular or *hemodynamic* changes are related to the electrical activity of neurons in a complex and delayed way. Local changes in the level of oxygenation reveal the active areas, but it is not possible to completely recover the electrical processes from the vascular ones. The hemodynamic changes are hard to model, but as their nature is somewhat slow and smoothly varying, a Gaussian model is often used. Some newer models of the hemodynamic response function are actually based on measurements from the real brain.

Usually, fMRI studies use a controlled stimulus, like visual patterns or audible beeps, designed to test a specific hypothesis. The simplest way of doing this is to repeat the stimulus several times, with resting periods in between, and scan the fMRI sequence during the whole time. Such experiments should reveal areas of the brain that are always active during the stimulation and inactive during the resting. Sometimes the subject can even be asked to perform a relatively simple mental or motor task during the scanning. Naturally, such tasks should not be allowed to result in head movement.

The low resolution and the scanning parameters, optimized for BOLD, make the contrast between different tissue types very poor. Additionally, the fast scanning and low signal-to-noise ratio of the BOLD signal make the image very noisy. Therefore, a high resolution structural MRI is often scanned separately to aid in locating the activation during analysis by superpositioning. The bright areas in the images do not necessarily correspond to the active ones. Careful analysis of the whole sequence is required to detect the activation patterns.

Knowledge of both the hemodynamic response function and the correlation structure of the noise is essential for this analysis. In medicine, it is common practice to use a fixed "standard" HRF to analyze data obtained from different subjects, different brain areas and different scans (acquired at different times). Commonly used HRFs are a Poisson function [4] or a gamma function [8] [9] [10]. However, it has been reported that observed HRFs seem to vary both spatially and temporally and also from subject to subject [11], [12], [13], [14]. If this observation were true, the use of one standard HRF would result in suboptimal test power and most likely in invalid inference. Furthermore, current methods deal with temporally correlated noise by pre-whitening the data based on the estimated correlation

matrix of the noise [15]. This correlation matrix is usually estimated by fitting an autoregressive (AR) time series model to the residuals obtained after fitting the general linear model to the fMRI time series in least squares sense [16]. Unfortunately, this "two-step approach" introduces a bias [17] [18] introduce a Bayesian approach that allows for an adequate pixelwise modeling of the hemodynamic response, and demonstrate the flexibility of the Bayesian model applying it to conditions of altered hemodynamics in a patient with cerebral arteriovenous malformation.

The convolutions account for a time delay and smooth increase of the blood flow. The methods to determine these functions range from preset values for the HRF parameters [6] over global estimates up to pixelwise solutions [19] [20] [21]. For pharmacologic BOLD experiments [22] propose a so-called waveform analysis protocol and model the hemodynamic response directly. Signal increase and decrease are described by two independent functions. Thus, a greater flexibility is achieved. However, in recent years, there is an increasing interest to explore the physiologic nature of the BOLD signal response and its dependence on the duration and type of neuronal stimulus. Knowledge about the characteristics of the HRF can help to understand the nature of the neurovascular coupling.

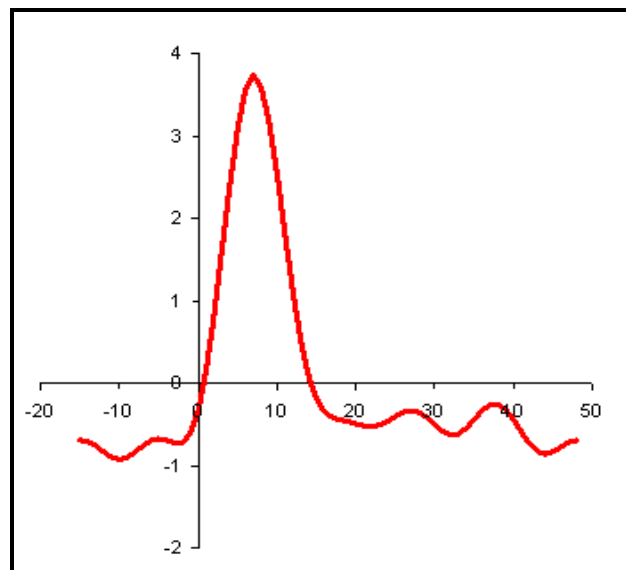


Figure 3.1. An example of HRF projected using Benar method, from a time scale of -18 seconds prior to the event to 48 seconds after the event

It is sometimes useful to project an HRF to examine the exact time course of the BOLD response, to a neuronal event. Use a Fourier basis method to calculate the HRF [23], in which a number of Fourier basis functions are applied to a time window to determine the shape of the HRF response. Many software packages, such as AFNI and SPM include the ability to examine the BOLD time course associated with an event.

### **3.2. Standard Preprocessing of Images**

In addition to the low signal-to-noise ratio and additive noise, the fMRI measurements are contaminated with artifacts, such as head movement and physiological vascular changes. Thus, the detection and analysis of interesting phenomena is very difficult. To overcome these difficulties, the images need to be preprocessed. The level of noise is reduced and the values are much more continuous. Also, the excess area outside the brain has been removed. The usual steps of the preprocessing include:

Retiming the slices to account for the fact that each slice was scanned at a slightly different time: Since the scanning is not instantaneous this kind of temporal smoothing improves the continuity of the measurements.

Realigning the slices to reduce head movement related artifacts. This makes the voxels of different time points match spatially and removes some of the empty area surrounding the head in the images.

Smoothing or low-pass filtering to reduce high frequency noise and to increase local voxel correlations: This increases the signal-to-noise ratio of the hemodynamic effect and makes detection of interesting phenomena easier.

Normalizing the volumes into a standard coordinate system; This allows comparing different scans and identifying known locations.

The normalization step is not required for analysis, but is often done to match the functional volumes to the structural ones. Additionally, the normalization makes comparisons between different subjects easier. In practice, this may somewhat distort the

brain in the images and individual differences may still remain quite big, so that caution needs to be taken when drawing inter-subject conclusions.

### 3.3. Standard Analysis of fMRI Sequences

The standard way of analyzing an fMRI sequence is to use statistical parametric mapping (SPM), which is based on a general linear model (GLM) the analysis reveals the areas of the brain that most probably fit a given hypothesis, which is presented as a reference time-course.

The reference time-course can be approximated using the stimulation pattern and a model of the hemodynamic response. This can be a repeated on-off type of stimulus. The stimulation time-course is then convolved with the model of the hemodynamic response, assumed Gaussian in the illustration.

The analysis can be considered in two steps. First, the reference time-course is compared to the time-course of each voxel in the fMRI sequence statistically. This produces an image of the probability to fit the given time-course, where the voxels with the highest probabilities are considered to be active. However, the probability image is very noisy and the second step is to segment it into the inactive and active areas. The segmentation is made by using a statistical model for the noise, usually assumed Gaussian. (The difficulty with this approach is to define a threshold for the probability of activation that produces an accurate segmentation. Choosing a too high value easily leads to discontinuous or too small areas. On the other hand, a small value may produce big areas that do not accurately locate the activation of interest).

After the spatial activation patterns have been formed, the true activation time-course of each area is formed by taking the mean sequence of all the voxels in the area. Again, if the segmentation is poor, for example, due to an incorrect threshold value, the time-courses are not generated accurately.

There are big problems with such analysis. The accuracy is limited by the ability to approximate the parameters needed for the statistical fitting. Also, small changes to the

parameters can change the results severely. Additionally, the stimulation setup has to be simple enough to allow predicting the responses, and forming the reference time-courses, in the first place. Therefore, detecting previously unknown phenomena is extremely hard and current research focuses on more data-driven and adaptive methods, like independent component analysis (ICA) and blind source separation (BSS). [24]

### **3.4. Combined EEG-fMRI Analysis**

Recent research has also focused on combining EEG and fMRI to study epilepsy. Epileptic activity is visible in the EEG in the form of prolonged discharges accompanying clinical seizures and interictal spikes, short events without clinical accompaniments. In epileptic patients, and particularly in those suffering from medically intractable seizures, it is important to record such events and to find which part of the brain generates them. This information helps classify the type of epilepsy and therefore administer optimal medical treatment. When medical treatment fails, it is possible to consider the surgical removal of epileptic brain tissue, provided this tissue can be accurately localized and provided it is not critical for normal brain function.

Combined EEG-fMRI methods are used to examine interictal events. EEG is recorded in the MRI scanner during the acquisition of functional scans. The EEG allows us to determine the timing of epileptic events and to examine the fMRI activation at that time. Recording EEG during fMRI scanning is very difficult, but some researchers worked out a meticulous setup to optimize EEG quality [25].

The patient has electrodes fixed to their head outside of the scanner using a conductive paste. When the patient enters the scanner, the electrodes are connected to an amplifier in the scanner room, which is in turn connected to a computer outside the scanner room via a fiber optic cable. The strong magnetic field in the scanner environment has a detrimental effect on the quality of the EEG. During fMRI scan acquisition, the RF pulse creates an artifact that completely obscures the EEG. It is then necessary to filter the EEG after the scanning session.

An experienced epileptologist reviews the EEG, indicating the timing of the spikes.



In this kind of study, one is interested in interictal events (spikes that are not part of a seizure) rather than ictal events. It is difficult to capture a seizure during the limited (2 hour) scan time, and any movement that occurs during the seizure may blur the image to such a degree that it becomes useless. Knowing the timing of the spikes (the events) and the timing of the MRI scans allows us to examine the fMRI signal at that time to look for responses related to the event.

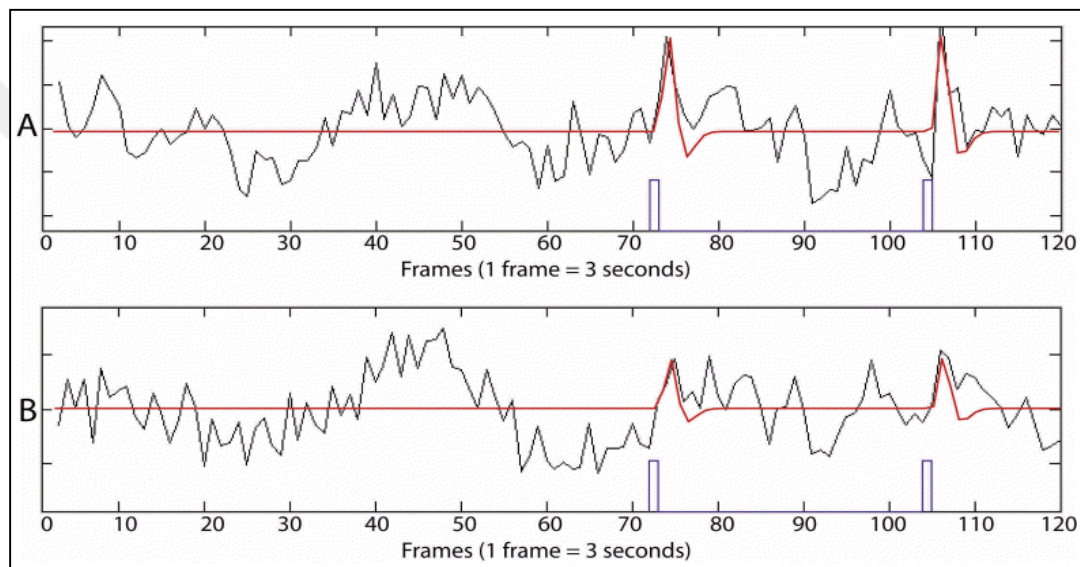


Figure 3.2. Examples of BOLD signal in a single voxel (5x5x5mm of brain tissue) during a 6 minute scan of 120 measurements (frames). The pulse marks show the approximate timing of an interictal EEG event, and the bold-font line shows an approximation of the model used to analyze the data. In part A the BOLD change to the EEG event is very clear and distinct. In part B, the change is smaller, but still noticeable by the naked eye. The voxel represented by part A has a stronger activation than part B. The signal is not always as clear as in this example

Once the timing of the events has been determined, the fMRI signal is analyzed. A number of runs (usually 10 to 14) are recorded. Each run has 120 scans of 25 slices (5mm x 5mm x 5mm voxels) that usually covers the entire brain, and takes 6 minutes to complete. A typical scanning time, including setup and anatomical scans, is 2 hours. Prior to analysis, any movements the patient may have made are corrected. With the event timing, the fMRI activity at that time to look for activation is examined. The fMRI signal is

referred to as the BOLD (blood oxygen level dependant) signal. The fMRI signal is not a direct result of neuronal firing, but a metabolic response based on increases in the deoxygenation of hemoglobin caused by neuronal activity. A neuronal event has an expected change in the BOLD signal (the hemodynamic response). To analyze the data, a model in which a pre-determined hemodynamic response function (HRF) is locked to the event timing is created. Thus, at every time in which there is an event there is a corresponding HRF. One then compares this model to the actual BOLD signal. If there is a good correspondence between the model and the signal, one has a response. Responses can be an increase (activation) or a decrease (deactivation).

Studies of focal epileptic spikes caused by different types of lesions were performed, as well as studies of the BOLD response to generalized epileptic discharges. Results show most often activations in the expected epileptic focus, but also often activations and deactivations at a distance. This remains at present a research tool and its clinical applicability is still uncertain.

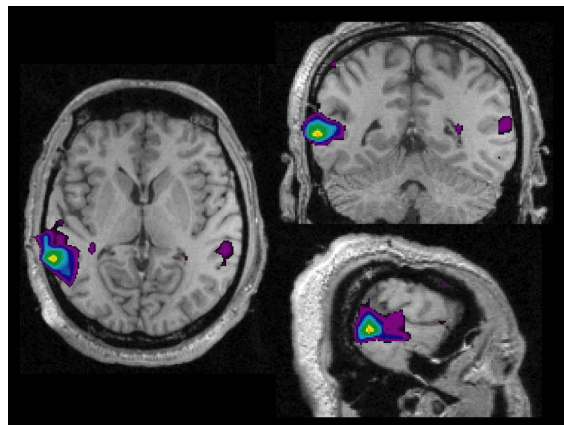


Figure 3.3. A statistical map of activation in a patient with left temporal spikes. Note the main area of activation on the left side, and the small activation in the contra-lateral area on the right

#### **4. A NON-FIBER OPTICAL SET UP FOR THE MEASUREMENT OF PATIENT RESPONSE TIME IN fMRI**

During brain activity there is a rapid momentary increase in the blood flow to the specific centers in the brain. This situation results in a corresponding local reduction in deoxyhemoglobin because the increase in blood flow occurs without an increase of similar magnitude in oxygen extraction. Since deoxyhemoglobin is paramagnetic, it alters the T2\* weighted magnetic resonance image signal. Thus, deoxyhemoglobin is sometimes referred to as an endogenous contrast enhancing agent, and serves as the source of the signal for functional magnetic resonance imaging, fMRI. Using an appropriate imaging sequence, human cortical functions can be observed without the use of exogenous contrast enhancing agents. The fMRI received considerable interest in clinical applications of neurophysiology and engineering. It is also a promising technique to demonstrate neuronal activity of the spinal cord, as it is performed in a noninvasive way. Thus the technique may have important clinical uses, for example in the rehabilitation of spinal cord injuries.

The main advantages of fMRI as a technique to image brain activity related to a specific task or sensory process include 1) the signal does not require injections of radioactive isotopes, 2) the total scan time required can be very short, i.e., on the order of 1.5 to 2.0 min per run (depending on the paradigm), and 3) the in-plane resolution of the functional image is generally about 1.5 x 1.5 mm although resolutions less than 1 mm are possible.

Recently, software packages for the analysis and visualization of functional and structural magnetic resonance imaging data sets have been introduced. Such programs run on all major computer platforms (e.g., Brain Voyager, Netherlands; MEDx software, Sensor Systems, Sterling, Va).

Although most fMRI examinations in routine practice employ simple patient response methods such as finger tapping, in modified fMRI examinations where the correspondence between performance and brain activation is studied, some additional instrumentation, like “patient response switch (PRS), interface and recorder” is required.

Throughout PRS based fMRI instrumentation patient reaction times can be measured and data can be correlated with other fMRI findings. For example, a correspondence between performance and brain activation for mental arithmetic has shown that patients with lesions in the inferior parietal lobe fail to perform simple number calculations. Recent studies involving healthy subjects and using hemodynamic neuroimaging methods demonstrate that inferior parietal and prefrontal cortical areas are activated during tasks that involve mental arithmetic [26] [27]. In an fMRI study involving PRS by Hugdahl et.al.[26], the comparison (normal) subjects had significantly shorter reaction times during the mental arithmetic task than did the patients with schizophrenia but not the patients with depression. No significant difference in reaction time was found between the patient groups.

A Fiber Optic Button Response System (FO-PRS) mainly consists of fMRI Button Response unit (e.g., Psychology Software Tools, Pittsburgh, PA) with MR Projection System. The Fiber Optic Button Response System is an fMRI ready subject response collection system which has been engineered to gather subject responses and verify signals.

The Fiber Optic Button Response Units attach to the subject's wrists and can be adjusted during scanning. These units are completely fiber optic, and connect to a fiber Optic Interface Console located in the control room through an available wave guide. The interface console provides real-time feedback of subject responses via LED indicators and includes a set of switches which can be used to make responses for the subject as needed. The system provides TTL output signals that can be used to interface with other data collection devices and software. The interface console comes with a RF Pulse that the computer interprets as another button press, allowing the user to synchronize their experiments with the MR scanner.

Such a commercially available standard unit comes with some cables, and provides serial port and USB connection to the data collection computer. However, an additional waveguide is required between the patient room and the operating room. On the other hand, existing wave-guide channel may not be employed, since it may already be crowded with the earlier installed cables or the length of the supplied cables can be too short to

provide the required connection. These difficulties prevent the practical use of such a technique, or require hiring of expensive skilled labor for extra cable installation, isolation and RF shielding.

There exist intensive electromagnetic signals generated by gradient and RF coils (during an fMRI examination, in particular). In addition, there is a strong constant magnetic field (as high as 3 Tesla) within the patient room, and at first glance, optical signal processing may seem to be reasonable to avoid distortions in such an environment. However, in this study, we show that relatively expensive fiber optical unit and fiber optical interface can be replaced by simple electronics without any disturbance to stimulus measuring unit as well as to the MRI. The cost of the measuring and interface unit whose performance has been reported in this work is very low as compared to commercially available equipment. This mainly stems from the fact that it consists of only few discrete electronic components, including a MOS transistor operating in switching mode.

#### **4.1. Materials and Methods**

The fMRI-PRS system described in this work is developed for fMRI experiments suitable for a 3 Tesla MRI and tested in a Philips, Intera Achieva unit. In this system, there is an “RF blocking” window glass partition between the patient room and MR control room, providing the technician to see the patient continuously. The window consists of a precisely aligned RF screen mesh component, sealed between layers of laminated safety glass and mounted in a special extruded frame for installation in the RF shielded wall. The frame electrically connects the RF shielding mesh in the window to the RF shielded enclosure itself. A special clamping extrusion holds the individual window units in place, forms the RF seal. The patient room is fully RF shielded with “mu-metal” material. Patient response measurement and interface unit is based on a visual stimulus and response paradigm, and consists of the following parts: a response button (non-ferromagnetic micro switch), the cable providing the communication between the response button and the optical interface (the transmitter circuit in the patient room, the receiver circuit in the operator room), a cable providing the communication between the receiver circuit and DAQ card (National Instruments, DAQmx), a cable with snap-on noise suppression ferrite (NI-USB 6501) providing the communication between DAQ card and the computer , the

projection device (Epson, Japan) and an in-house manufactured non-metallic semi-transparent screen. Various images are projected onto a transparent screen. The projection device resides in the MR control room and the patient sees the images on the projection device over a 45 degree tilted mirror which is placed on the Head Coil used during fMRI examination. The patient is trained by the MTA so that he or she presses the button in response to the images projected on this screen in the magnet room during fMRI examination.

The block diagram of this system is shown in Fig 4.1.

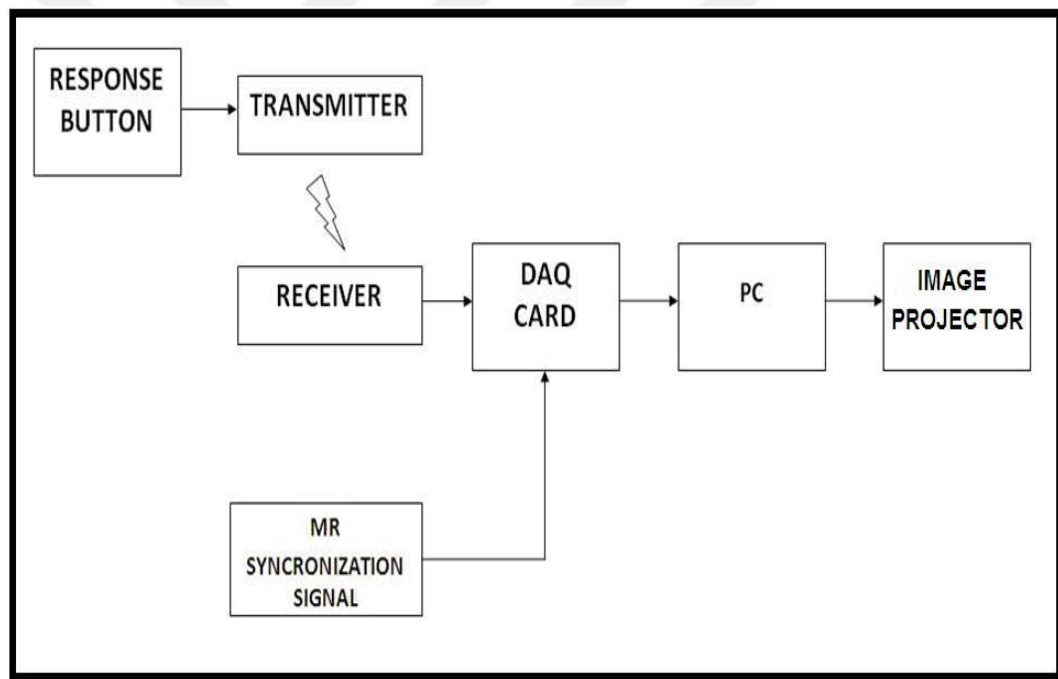


Figure 4.1. Block diagram of the patient response measuring system

Signal coupling is accomplished via the optical interface unit which is placed between two sides of the RF shielded glass window. These parts look alike in the form of conic horns. In order to provide an efficient signal coupling between the receiver and the transmitter, a 2.5 V /0.3 A miniature light bulb with a lens has been adapted in the transmitting cone. Due to double glass structure of the RF screen window, the distance between the receiver and the transmitter is large enough to cause stray light to interfere the

signal from transmitter cone. This stray light originates mainly from the projector and the operating room lighting although the latter is dimmed. Therefore this stray light needs to be blocked. Additionally, both the transmitting and receiving cones were enclosed by multiple wound aluminum foil to increase the scattered and stray light immunity of the system, Fig.4.2.1, 4.2.2. Both cones are of plastic material. The receiver cone in the operating room is located on the same window, exactly positioned across the transmitter cone. Both cones are gently fixed on the window glass using an opaque scotch tape. Patient response button is fixed firmly onto the patient couch. The connection between the patient button and the transmitter circuit consists of about 3 meters of twisted line pair so laid to eliminate any loops around the patient table. Similar but shorter line pair is used between the receiver board and the computer interface. Fig.4.3 and Fig.4.4 show image projector and receiver electronics, and image display screen, respectively.

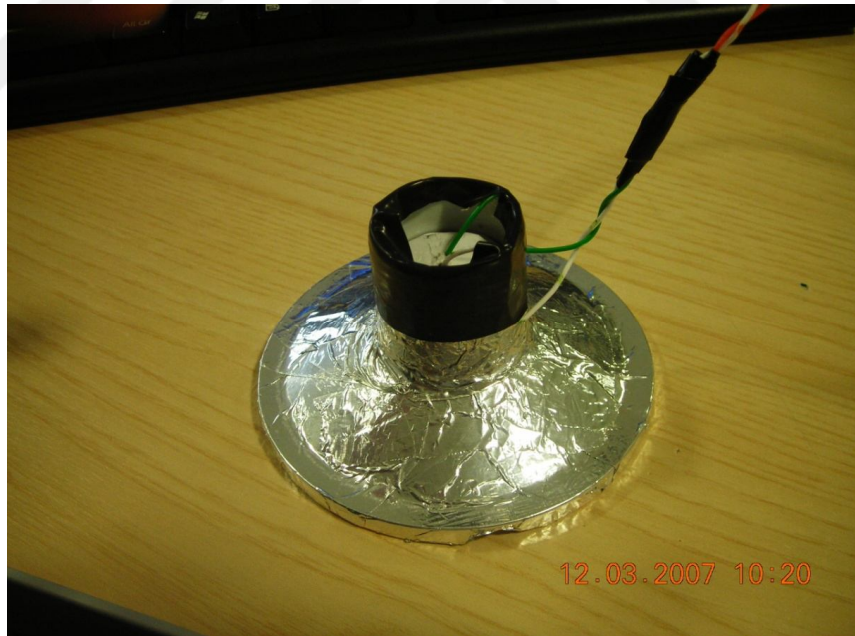


Figure 4.2.1. Transmitter cone

#### 4.1.1. Circuit

Complete optical interface electronics is shown in Fig 4.5. In this circuit, the switch S1 is a miniature snap-action type. (This kind of switch offers long operating life. With

multiple options available for contact configurations, terminals and actuators, one can configure a miniature snap-action switch to fit nearly any sizes. In our experiments this switch has been slightly modified). It is normally off (non-conducting). When depressed, a small current ( $4\ \mu\text{A}$ ) flows through the switch and connects the gate of transistor Q1 to supply voltage ( $V_{cc}=9\text{V}$ ). Since it is in source follower configuration, the voltage pulse at its source terminal follows the gate pulse. (See, Fig. 4.7 and Fig. 4.8). This voltage is transmitted to the base of Q2 through R3 and R4. (Here, R4 is fixed resistor at  $3.9\ \text{k}\Omega$ , while R3 is used for best adjustment of total base resistance. It has been experimentally observed that best operation is reached when it has  $1\ \text{k}\Omega$  value. Then the potentiometer was replaced with a fixed resistor of the same value).

The term “best operation” is used here for the condition that activates the lamp (Lx) and the photo-resistor (Rx) pair through the viewing glass in the MRI control room.

The receiver is a simple bipolar transistor switching circuit. Here, the collector of transistor Q3 is normally at high level, but when the light activates the photo resistor, transistor saturates and brings the collector voltage into low level. This triggers an active pulse for DAQ board. (Fig.4.9, Fig. 4.10 and Fig. 4.11)

Figures 4.12, 4.13 and 4.14 demonstrate the test set up.

The receiver circuit is connected to data acquisition (DAQ) card and the DAQ card is connected to the computer as shown in Fig. 4.6. MR synchronization output is readily available on the unit (in the operation room) and that TTL compatible signal is also fed to computer via DAQ card. Therefore, EPI sequence and timing of the events are well synchronized.

A  $60\ \mu\text{s}$  wide TTL compatible MR SYNC pulse is derived from the user interface of the MRI unit which is located in the operating room. This signal is fed to (DI 2) digital input of DAQ board so that it is activated on the rising edge of the pulse. Another TTL output signal derived from the patient response interface is connected to other digital input (DI 1) terminal of DAQ board. DAQ board is configured using software in C language.





Figure 4.2.2. Transmitter cone, front view

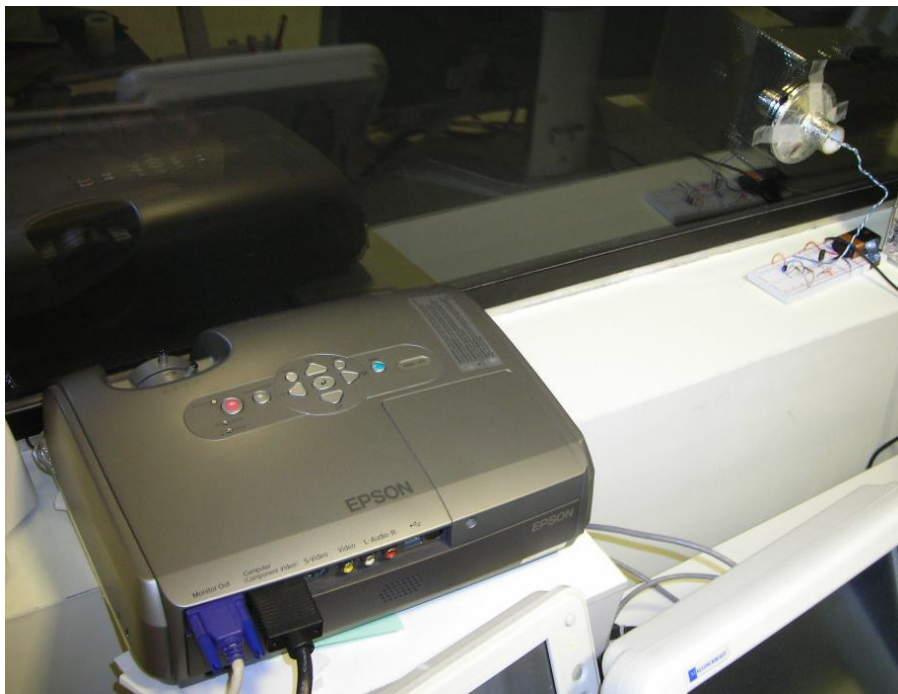


Figure 4.3. Image projector, the receiver sensor and electronics (upper right) in the operating room



Figure 4.4. Semi-transparent image display screen

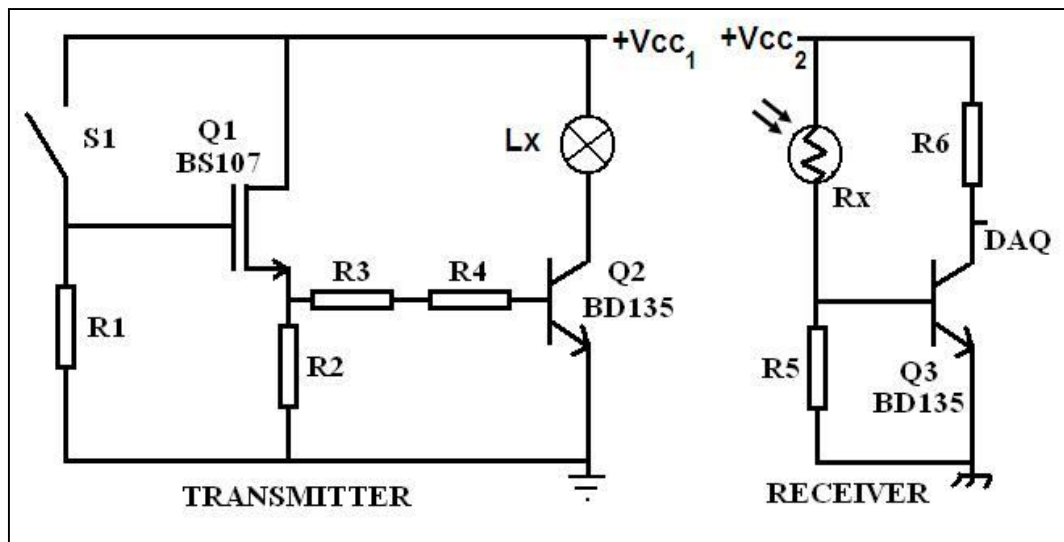


Figure 4.5. The patient response circuit

$R1=2.2M$ ,  $R2=120$ ,  $R3=1k$ ,  $R4=3.9k$ ,  $R5=470k$ ,  $R6=2.2k$ ,  $Q1=BS107$ ,  $Q2=BD135$ ,  $Q3=BD 135$ ,  $R_x=Photo\ resistor$ ,  $V_{cc1}=V_{cc2}=9V$  with separate grounds, DAQ output feeds DI1 terminal of the data acquisition circuit.

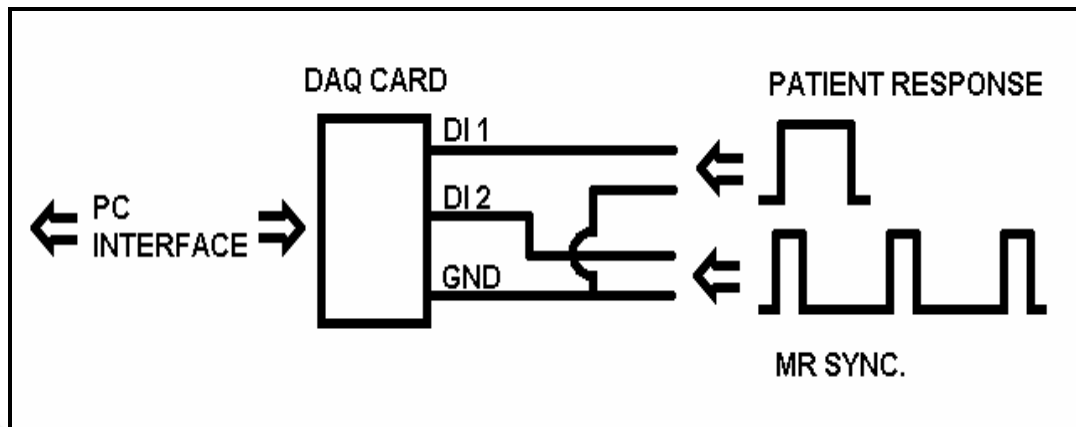


Figure 4.6. Computer interface circuit using DAQ card (National Instruments, DAQmx)

This program simultaneously detects rising edges of both digital input signals, and performs the required jobs, accordingly. While visual stimuli are controlled in accordance with the fMRI paradigm using MR SYNC pulses, patient response pulses avails the measurement of patient response time to visual excitation.

#### 4.2. Mutual Interaction Tests:

Experimental verification of non-interaction between the interface unit and the MRI system was validated by successive turning on and off the patient switch during a BOLD fMRI sequence using a bottle phantom scanning. Here, a water phantom was used and its circular cross-sectional images were recorded, then post processing of rectangular (region of interest) areas were statistically evaluated. The statistical parameters of these ROIs did not change when the switch is operating and not operating condition. Therefore, it can be concluded that the transmitter part of the patient switch response unit does not interfere with the MRI.

On the other hand, very strong gradient field effect was readily observed on the patient response circuit. This is expected for most MRI sequences, however, such an electromagnetic interaction is more pronounced during BOLD-fMRI, as the magnetic field gradient strength is much higher than the other MRI sequences with longer durations. In that sense, design of the transmitter part of the fMRI patient response circuit was quite

challenging. Strong gradient pulses induce a voltage in the transmitter so that a “false trigger” signals results at the output of the optical interface circuit, although the patient response switch was not in depressed position. It has been noted that practically no EMI-shielding measures were capable of reducing this effect, perfectly. Finally, transmitting part of the circuit has been so designed that a signal appears at the output only if the patient switch is momentarily closed, while induced RF and gradient pulses on the circuit do not create any problems. In addition, by adjusting the trigger threshold level, continuous depression of the patient switch does not constitute a problem. Nevertheless, (before test procedure is initiated) patients or subjects need to be instructed not to depress the button for long duration.

#### **4.3. Additional remarks**

Although visual stimulation was used a means of generating a patient response during our fMRI experiments, other forms of stimuli (audio, heating, touching, etc..) could also be used, as the response circuit is independent part of the fMRI experiment.

This proposed set up does not employ any light emitting diodes (LEDs) in the interface circuit. Because a small incandescent light bulb is used in transmitter part attached onto the glass window which separates operating room and magnet room, some time delay at the order of a few milliseconds is introduced at the receiver output from the time patient response switch is activated. Although a LED could be thought as an alternative (which could reduce the encountered time delay), it has been observed that the window glass significantly decreased the intensity of light due to its special construction. This precludes the use of low current-low intensity LED application. Note that increased sensitivity of the receiver electronics does not improve the delay time, because of reflection and stray light problems on the window structure. Nevertheless, from the clinical point of view, this delay time is found to be tolerable (negligible) as compared to overall (subject) response time. This is illustrated in Table 4.1.

Transmitter part of the proposed circuit can be improved by adding a monostable section, so that, even if the patient response button is held in depressed position, no

disturbances may occur. However, this happens very rarely, therefore such a modification was not applied to the circuit during the fMRI experiments.

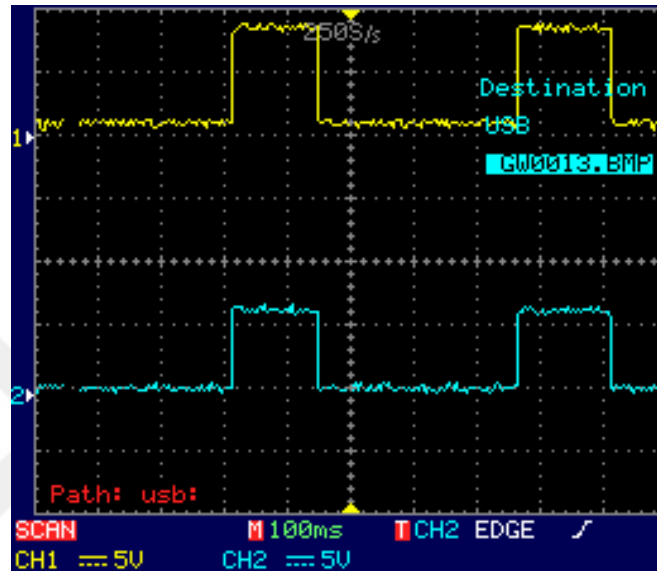


Figure 4.7. Transmitter side, voltage pulses at the gate of the MOSFET (upper trace, CH1) and the base of BJT (CH2)

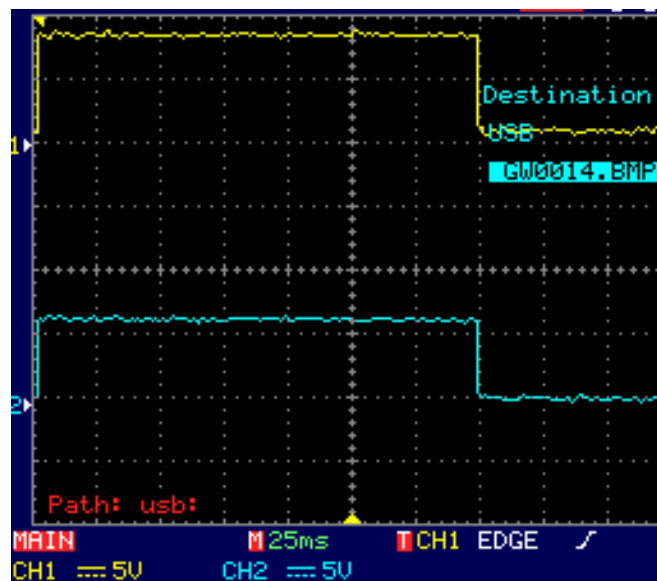


Figure 4.8. Transmitter side expanded time scale view of voltage pulses at the gate of the MOSFET (upper trace, CH1) and the base of BJT (CH2)

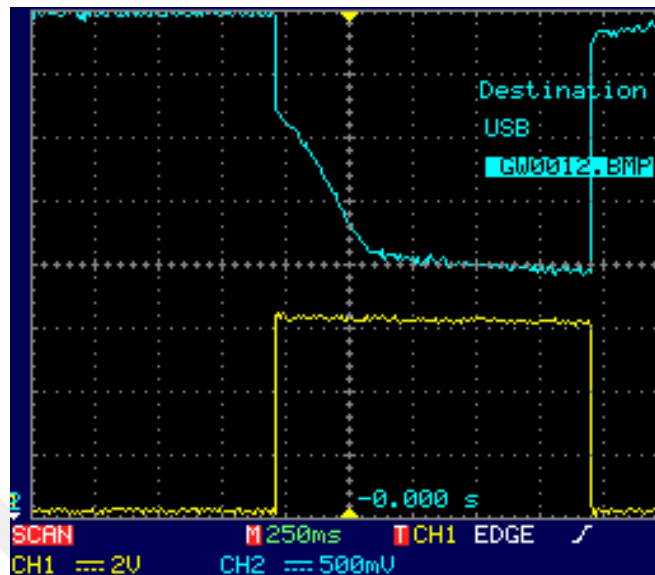


Figure 4.9. Transmitter side voltage pulses at the gate of the MOSFET (CH1) and the collector of BJT (CH2). This record demonstrates the time delay caused by incandescent mini-lamp

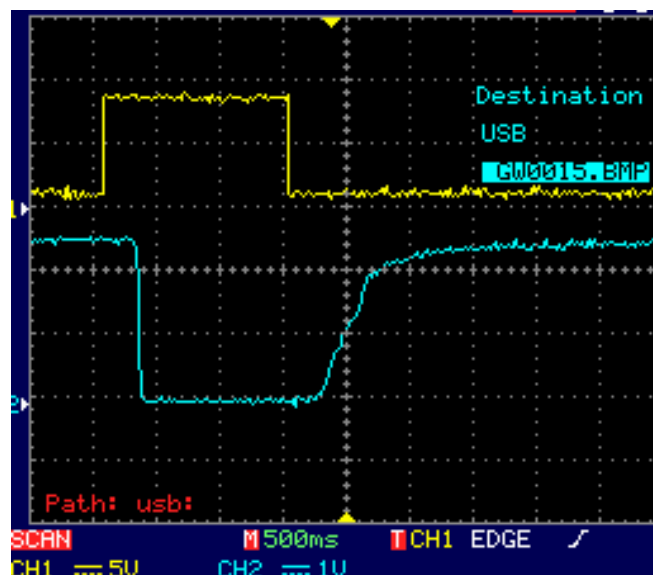


Figure 4.10. The overall response. Upper trace (CH1) is the voltage pulse at the gate of the MOSFET due to closed switch action, while the lower trace (CH2) shows the signal at the input of DAC card (output of receiver unit). Rising edge of the lower trace is mainly due to recovery time of photo-resistor element (from light to dark transition) which is not

considered here (Only the excitation edge of the receiver signal is significant for the analysis)

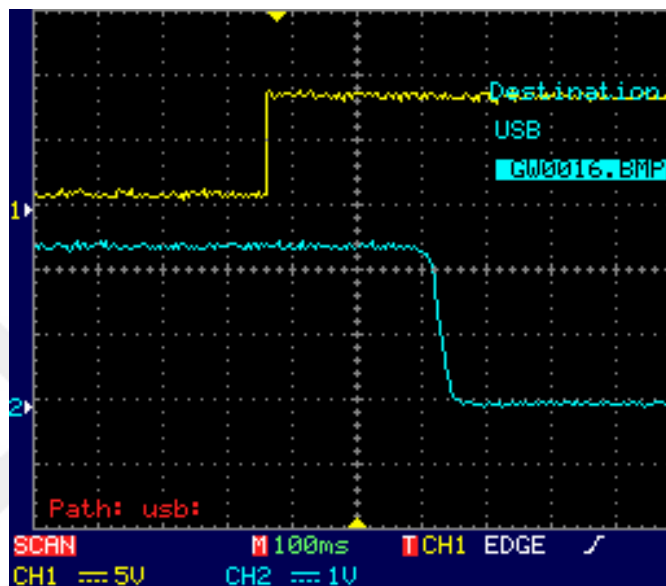


Figure 4.11. Time expanded view of Overall response. Upper trace (CH1) is the voltage pulse at the gate of the MOSFET due to closed switch action, while the lower trace (CH2) shows the signal at the input of DAC card (output of receiver unit). Total electro-optical time delay can be compensated by software

Table 4.1. Reaction Time of Patients with Schizophrenia or Major Depression and Healthy Comparison Subjects for a Vigilance Task and Mental Arithmetic Task Kenneth Hugdahl et.al, Brain Activation Measured With fMRI During a Mental Arithmetic Task in Schizophrenia and Major Depression, Am Psychiatry 2004; 161:286-293

Reaction Time (msec) <sup>a</sup>					
Patients With Schizophrenia (N=12)		Patients With Depression (N=12)		Comparison Subjects (N=12)	
Mean	SD	Mean	SD	Mean	SD
564	167	481	134	501	118
691	186	622	143	596	148

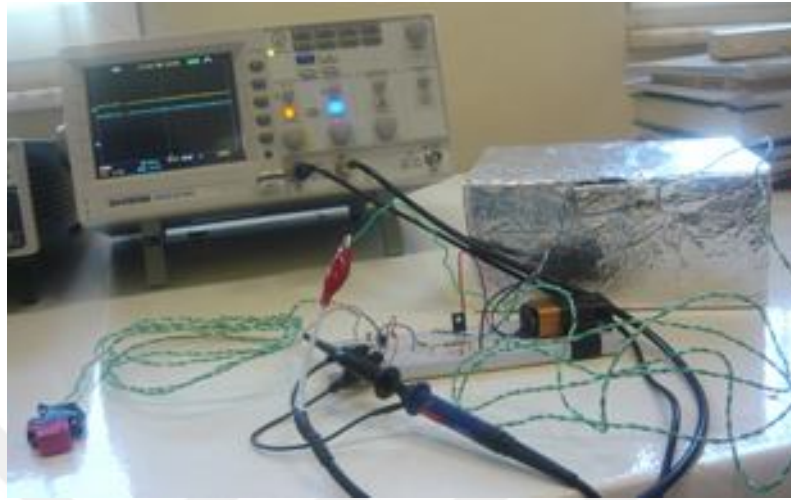


Figure 4.12. Experimental set up for measuring intrinsic electro-optical time delay

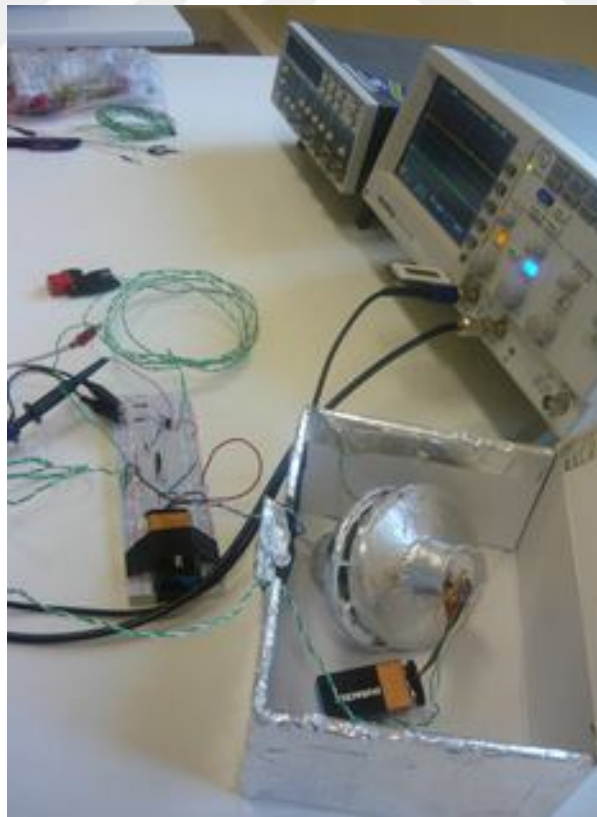


Figure 4.13. The dark box is covered with an aluminum adhesive tape and electrically grounded





Figure 4.14. Receiver, printed circuit board and transmitter cones in the light isolation box

## 5. CONCLUSION

This thesis presents a brief review of “Magnetic Resonance Imaging” (MRI) physics fundamentals and imaging sequences followed by a description of the “Functional MRI” (fMRI). The last chapter introduces a device to be used in fMRI which is useful in measuring and recording patient’s response time in a related fMRI examination. The proposed method is a simple and low cost “patient response set up” which does not involve fiber-optics based sensors. The performance of the proposed measurement set up is tested using fMRI sequences in a 3 Tesla MRI unit, and it works quite efficiently.

Some clinical studies which employ this set up are under way and their results will be reported elsewhere in near future.

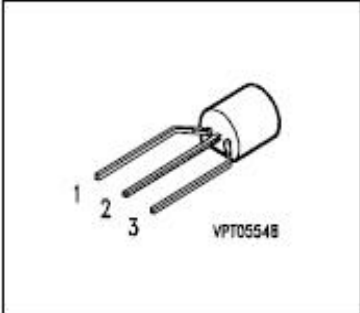
## REFERENCES

1. J.P.Hornak, The basics of MRI. [Cis.rit.edu/htbooks/mri/inside.htm](http://Cis.rit.edu/htbooks/mri/inside.htm)
2. Schneider, W., Casey, B., and Noll, D. 1993. Functional MRI mapping of stimulus rate effects across visual processing stages. *Hum. Brain Mapping* **1**:117–133.
3. Worsley, K. J., Evans, A. C., Marrett, S., and Neelin, P. 1992. A three-dimensional statistical analysis for CBF activation studies in human brain. *J. Cereb. Blood Flow Metab.* **12**:900–918
4. K. J. Friston, A. P. Holmes, K. J. Worsley, J. B. Poline, C. D. Frith, and R. S. J. Frackowiak, Statistical parametric maps in functional imaging: a general linear approach, *Hum Brain Mapp*, vol. 2, pp. 189-210, 1995.
5. Bandettini, P. A., Jesmanowicz, A., Wong, E. C., and Hyde, J. S. 1993. Processing strategies for time-course data sets in functional MRI of the human brain. *Magn. Reson. Med.* **30**:161–173.
6. Friston, K. J., Holmes, A. P., Worsley, K. J., Poline, J.-B., Williams, S. C. R., and Frackowiak, R. S. J. 1994. Analysis of functional MRI time-series. *Hum. Brain Mapp.* **1**: 153–171.
7. M. S. Cohen, Real-time functional magnetic resonance imaging, *Methods*, vol. 25, pp.201-220, 2001.
8. V. Clark, J. Maisog, and J. Haxby, An fmri study of face perception and memory using random stimulus sequences, *Journal of Neurophysiology*, vol. 79, no. 6, pp. 3257-3265, 1998.
9. S. Courtney, L. Ungerleider, K. Neil, and J. Haxby, Transient and sustained activity in a distributed neural system for human working memory, *Nature*, vol. 386, 1997.

10. Dale and R. Buckner, Selective averaging of rapidly presented individual trials using fmri," *Human Brain Mapping*, vol. 5, pp. 329-340, 1997.
11. S. Kim, W. Richter, and K. Ugurbil, Limitations of temporal resolution in functional mri, *Magn Reson Med*, vol. 37, no. 4, pp. 631-636, 1997.
12. E. Zarahn, G. Aguirre, and M. D'Esposito, Empirical analysis of bold fmri statistics, *NeuroImage*, vol. 5, pp. 179-197, 1997.
13. G. Aguirre, E. Zarahn, and M. D'Esposito, The variability of human, bold hemodynamic responses, *NeuroImage*, vol. 8, pp. 360-369, 1998.
14. N. Lange and S. Zeger, Non-linear fourier time series for human brain mapping by functional magnetic resonance imaging (with discussion), *Applied Statistics*, vol. 21, 1997.
15. K. J. Worsley, C. H. Liao, J. Aston, V. Petre, G. H. Duncan, F. Morales, and A. C. Evans, A general statistical analysis for fMRI data, *NeuroImage*, vol. 15, pp. 1-15, 2002.
16. M. W. Woolrich, B. D. Ripley, J. M. Brady, and S. Smith, Temporal autocorrelation in univariate linear modelling of fMRI data, *NeuroImage*, vol. 14, no. 6, pp. 1370-1386, 2001.
17. J. Marchini and S. Smith, On bias in the estimation of autocorrelation in univariate linear modelling of fmri data, *NeuroImage*, vol. 18, pp. 83-90, 2003.
18. C. Goessl, L. Fahrmeir and D. P. Auer, Bayesian Modeling of the Hemodynamic Response Function in BOLD fMRI, *NeuroImage* 14, 140–148 (2001)
19. M. S. Cohen, Parametric Analysis of fMRI Data Using Linear Systems Methods, *Neuroimage* 6, 93–103 (1997)

20. Rajapakse, J. C., Kruggel, F., Maisog, J. M., and von Cramon, D. Y. 1998. Modeling hemodynamic response for analysis of functional MRI time-series. *Hum. Brain Mapp.* **6**: 283–300.
21. Goessl, C., Auer, D. P., and Fahrmeir, L. 2000. Dynamic models in fMRI. *Magn. Reson. Med.* **43**: 72–81.
22. Bloom, A. S., Hoffmann, R. G., Fuller, S. A., Pankiewicz, J., Harsch, H. H., and Stein, E. 1999. Determination of drug-induced changes in functional MRI signal using a pharmacokinetic model. *Hum. Brain Mapp.* **8**: 235–244.
23. Benar CG, Gross DW, Wang Y, Petre V, Pike B, Dubeau F, Gotman J. The BOLD response to interictal epileptiform discharges. *NeuroImage* 17:1182-1192, 2002
24. I. Atkinson, F. Kamalabadi, K. R. Thulborn, D. L. Jones, Blind estimation of fmri data for improved bold contrast detection, 3rd IEEE International Symposium on Biomedical Imaging, 6-9 April 2006 ,1056 – 1059.
25. C. Grova, J. Daunizeau, E. Kobayashi, A.P. Bagshaw, J-M. Lina, F. Dubeau and J. Gotman Concordance between distributed EEG source localization and simultaneous EEG-fMRI studies of epileptic spikes. *NeuroImage*, 39, 2, 2008, 755-774
26. K. Hugdahl, B. R. Rund, A. Lund, A. Asbjørnsen, J. Egeland, L. Ersland, N. I. Landrø, A. Roness, K. I. Stordal, K. Sundet, T. Thomsen, 2004, “Brain Activation Measured With fMRI During a Mental Arithmetic Task in Schizophrenia and Major Depression”, *Am J Psychiatry*, 161:286–293
27. Rueckert L, Lange N, Partiot A, Appollonio I, Litvan I, LeBihan D, Grafman J: Visualizing cortical activation during mental calculation with functional MRI. *Neuroimage* 1996; 3:97–103

## APPENDIX A: BS 107 TRANSISTOR DATA SHEET

<b>BS 107</b>											
<b>SIPMOS<sup>®</sup> Small-Signal Transistor</b>											
<ul style="list-style-type: none"> <li>• N channel</li> <li>• Enhancement mode</li> <li>• Logic Level</li> <li>• <math>V_{GS(th)} = 0.8...2.0V</math></li> </ul>											
											
<table border="1" style="margin-left: auto; margin-right: auto;"> <thead> <tr> <th>Pin 1</th> <th>Pin 2</th> <th>Pin 3</th> </tr> </thead> <tbody> <tr> <td>S</td> <td>G</td> <td>D</td> </tr> </tbody> </table>						Pin 1	Pin 2	Pin 3	S	G	D
Pin 1	Pin 2	Pin 3									
S	G	D									
<b>Type</b>	<b><math>V_{DS}</math></b>	<b><math>I_D</math></b>	<b><math>R_{DS(on)}</math></b>	<b>Package</b>	<b>Marking</b>						
BS 107	200 V	0.13 A	26 $\Omega$	TO-92	BS 107						
<b>Type</b>	<b>Ordering Code</b>		<b>Tape and Reel Information</b>								
BS 107	Q67000-S078		E6288								
<b>Maximum Ratings</b>											
<b>Parameter</b>	<b>Symbol</b>	<b>Values</b>	<b>Unit</b>								
Drain source voltage	$V_{DS}$	200	V								
Drain-gate voltage	$V_{DGR}$	200									
$R_{GS} = 20\text{ k}\Omega$											
Gate source voltage	$V_{GS}$	$\pm 20$									
ESD Sensitivity (HBM) as per MIL-STD 883		Class 1									
Continuous drain current	$I_D$	0.13	A								
$T_A = 31\text{ }^\circ\text{C}$											
DC drain current, pulsed	$I_{Dpuls}$	0.52									
$T_A = 25\text{ }^\circ\text{C}$											
Power dissipation	$P_{tot}$	1	W								
$T_A = 25\text{ }^\circ\text{C}$											

Maximum Ratings					
Parameter	Symbol	Values			Unit
Chip or operating temperature	$T_j$	-55 ... + 150			°C
Storage temperature	$T_{stg}$	-55 ... + 150			
Thermal resistance, chip to ambient air <sup>1)</sup>	$R_{thJA}$	≤ 125			K/W
DIN humidity category, DIN 40 040		E			
IEC climatic category, DIN IEC 68-1		55 / 150 / 56			

Electrical Characteristics, at $T_j = 25^\circ\text{C}$ , unless otherwise specified					
Parameter	Symbol	Values			Unit
		min.	typ.	max.	
<b>Static Characteristics</b>					
Drain- source breakdown voltage $V_{GS} = 0\text{ V}, I_D = 0.25\text{ mA}, T_j = 25^\circ\text{C}$	$V_{(BR)DSS}$	200	-	-	V
Gate threshold voltage $V_{GS} = V_{DS}, I_D = 1\text{ mA}$	$V_{GS(th)}$	0.8	1.5	2	
Zero gate voltage drain current $V_{DS} = 200\text{ V}, V_{GS} = 0\text{ V}, T_j = 25^\circ\text{C}$	$I_{DSS}$	-	0.1	1	μA
$V_{DS} = 200\text{ V}, V_{GS} = 0\text{ V}, T_j = 125^\circ\text{C}$		-	2	60	
$V_{DS} = 130\text{ V}, V_{GS} = 0\text{ V}, T_j = 25^\circ\text{C}$		-	-	30	nA
$V_{DS} = 70\text{ V}, V_{GS} = 0.2\text{ V}, T_j = 25^\circ\text{C}$		-	-	1	μA
Gate-source leakage current $V_{GS} = 20\text{ V}, V_{DS} = 0\text{ V}$	$I_{GSS}$	-	1	10	nA
Drain-Source on-state resistance $V_{GS} = 4.5\text{ V}, I_D = 0.12\text{ A}$	$R_{DS(on)}$	-	14	26	Ω
$V_{GS} = 2.8\text{ V}, I_D = 0.02\text{ A}$		-	14.5	28	

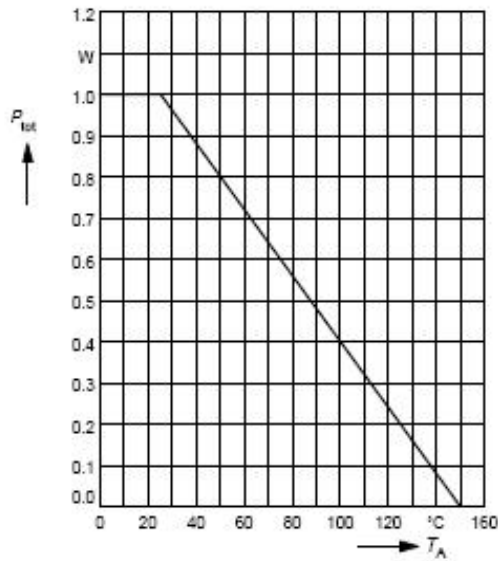
Electrical Characteristics, at $T_j = 25^\circ\text{C}$ , unless otherwise specified					
Parameter	Symbol	Values			Unit
		min.	typ.	max.	
<b>Dynamic Characteristics</b>					
Transconductance $V_{DS} \geq 2 \times I_D \times R_{DS(on)max}$ , $I_D = 0.12\text{ A}$	$g_{fs}$	0.06	0.17	-	S
Input capacitance $V_{GS} = 0\text{ V}$ , $V_{DS} = 25\text{ V}$ , $f = 1\text{ MHz}$	$C_{iss}$	-	60	80	pF
Output capacitance $V_{GS} = 0\text{ V}$ , $V_{DS} = 25\text{ V}$ , $f = 1\text{ MHz}$	$C_{oss}$	-	8	12	
Reverse transfer capacitance $V_{GS} = 0\text{ V}$ , $V_{DS} = 25\text{ V}$ , $f = 1\text{ MHz}$	$C_{rss}$	-	3.5	5	
Turn-on delay time $V_{DD} = 30\text{ V}$ , $V_{GS} = 10\text{ V}$ , $I_D = 0.24\text{ A}$ $R_G = 50\ \Omega$	$t_{d(on)}$	-	5	8	ns
Rise time $V_{DD} = 30\text{ V}$ , $V_{GS} = 10\text{ V}$ , $I_D = 0.24\text{ A}$ $R_G = 50\ \Omega$	$t_r$	-	8	12	
Turn-off delay time $V_{DD} = 30\text{ V}$ , $V_{GS} = 10\text{ V}$ , $I_D = 0.24\text{ A}$ $R_G = 50\ \Omega$	$t_{d(off)}$	-	12	16	
Fall time $V_{DD} = 30\text{ V}$ , $V_{GS} = 10\text{ V}$ , $I_D = 0.24\text{ A}$ $R_G = 50\ \Omega$	$t_f$	-	15	20	

Electrical Characteristics, at $T_j = 25^\circ\text{C}$ , unless otherwise specified					
Parameter	Symbol	Values			Unit
		min.	typ.	max.	
<b>Reverse Diode</b>					
Inverse diode continuous forward current $T_A = 25^\circ\text{C}$	$I_S$	-	-	0.13	A
Inverse diode direct current, pulsed $T_A = 25^\circ\text{C}$	$I_{SM}$	-	-	0.52	
Inverse diode forward voltage $V_{GS} = 0\text{ V}$ , $I_F = 0.5\text{ A}$	$V_{SD}$	-	0.9	1.2	V



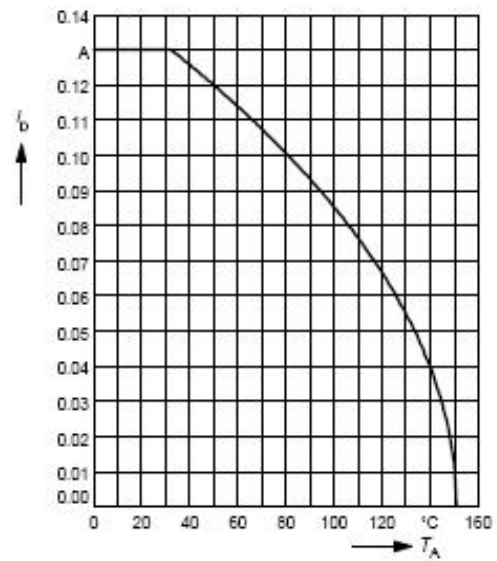
**Power dissipation**

$P_{tot} = f(T_A)$



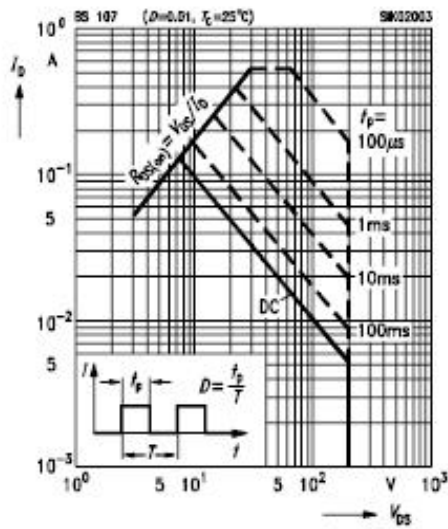
**Drain current**

$I_D = f(T_A)$   
parameter:  $V_{GS} \geq 4$  V



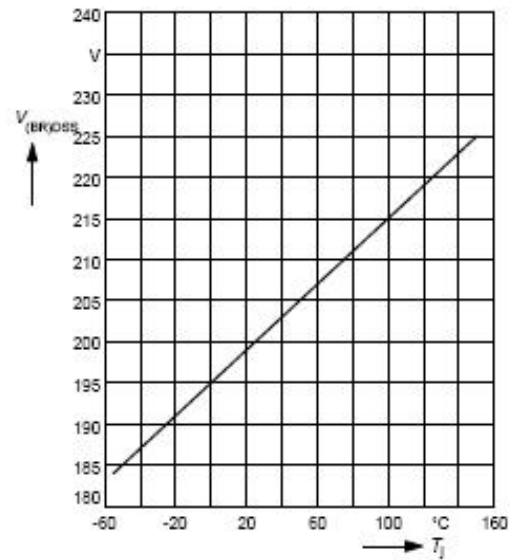
**Safe operating area  $I_D = f(V_{DS})$**

parameter:  $D = 0.01$ ,  $T_C = 25^\circ\text{C}$



**Drain-source breakdown voltage**

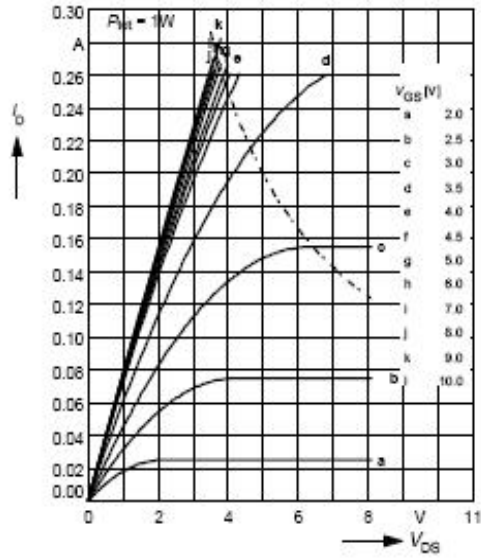
$V_{(BR)DSS} = f(T_j)$



**Typ. output characteristics**

$I_D = f(V_{DS})$

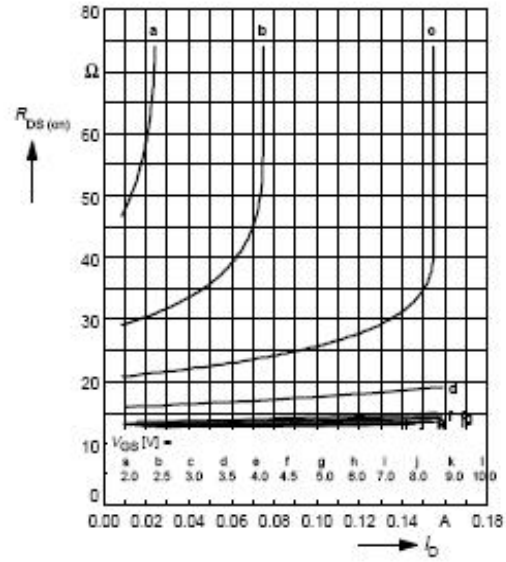
parameter:  $t_p = 80 \mu s$ ,  $T_j = 25^\circ C$



**Typ. drain-source on-resistance**

$R_{DS(on)} = f(I_D)$

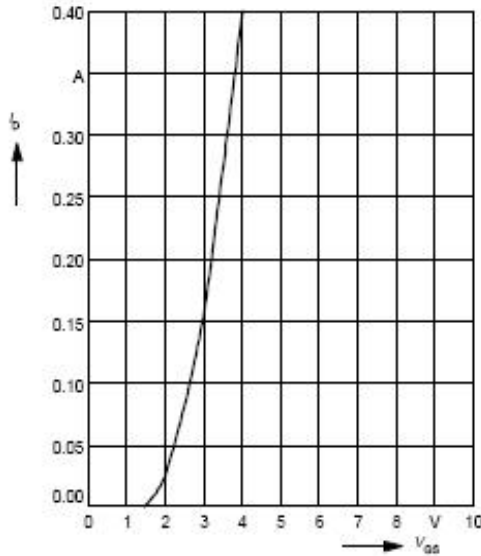
parameter:  $t_p = 80 \mu s$ ,  $T_j = 25^\circ C$



**Typ. transfer characteristics  $I_D = f(V_{GS})$**

parameter:  $t_p = 80 \mu s$

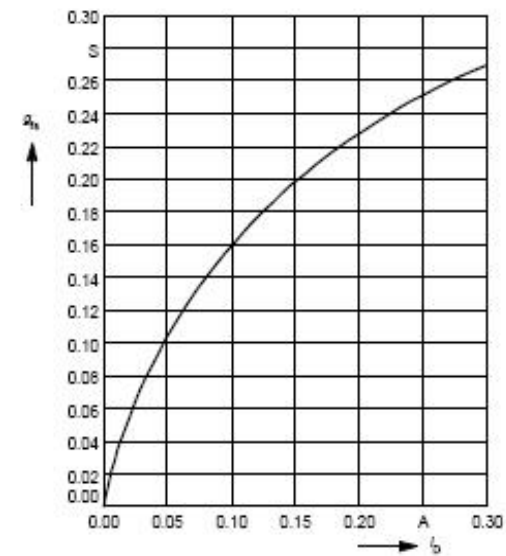
$V_{DS} \geq 2 \times I_D \times R_{DS(on)max}$



**Typ. forward transconductance  $g_{fs} = f(I_D)$**

parameter:  $t_p = 80 \mu s$ ,

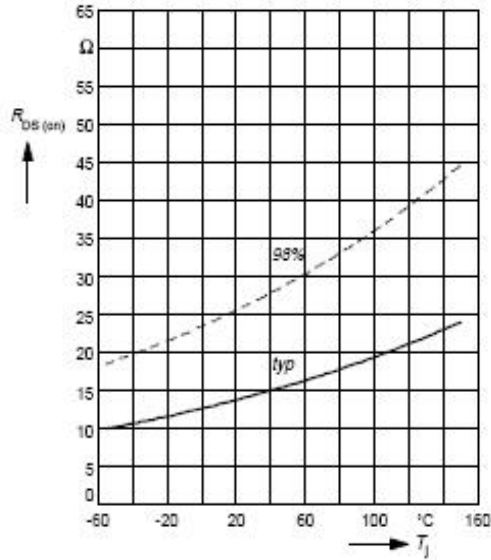
$V_{DS} \geq 2 \times I_D \times R_{DS(on)max}$



**Drain-source on-resistance**

$$R_{DS(on)} = f(T_j)$$

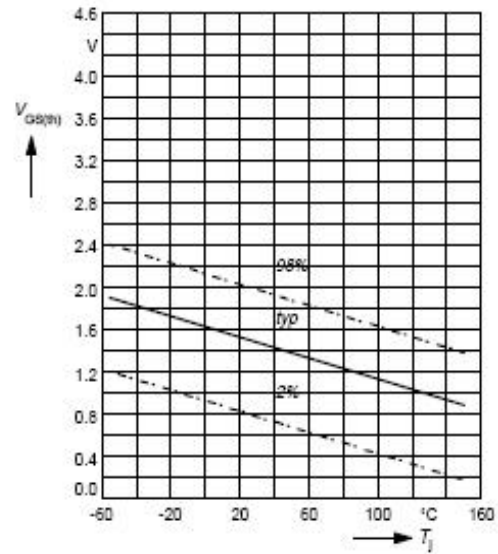
parameter:  $I_D = 0.12 \text{ A}$ ,  $V_{GS} = 4.5 \text{ V}$



**Gate threshold voltage**

$$V_{GS(th)} = f(T_j)$$

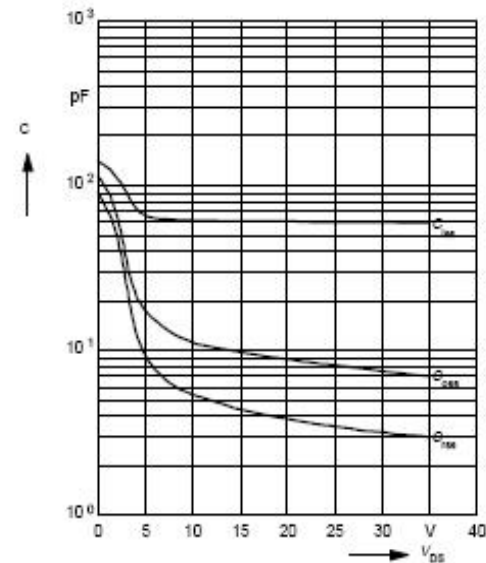
parameter:  $V_{GS} = V_{DS}$ ,  $I_D = 1 \text{ mA}$



**Typ. capacitances**

$$C = f(V_{DS})$$

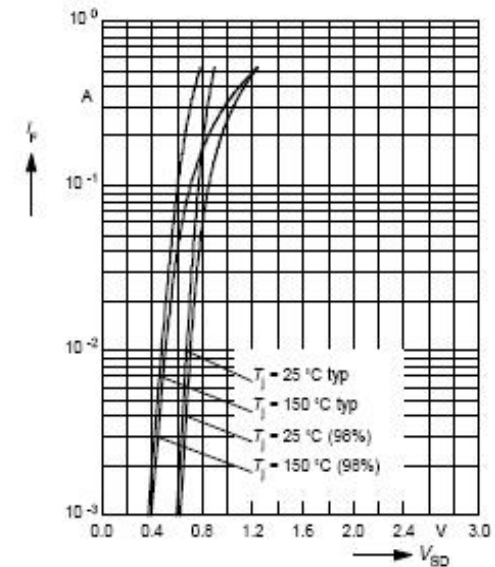
parameter:  $V_{GS} = 0 \text{ V}$ ,  $f = 1 \text{ MHz}$



**Forward characteristics of reverse diode**

$$I_F = f(V_{SD})$$

parameter:  $T_j, t_p = 80 \mu\text{s}$



## APPENDIX B: BD 135 TRANSISTOR DATA SHEET

### NPN SILICON TRANSISTORS

- STMicroelectronics PREFERRED SALESTYPES

#### DESCRIPTION

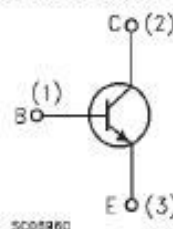
The BD135 and BD139 are silicon epitaxial planar NPN transistors in Jedec SOT-32 plastic package, designed for audio amplifiers and drivers utilizing complementary or quasi complementary circuits.

The complementary PNP types are BD136 and BD140 respectively.



SOT-32

#### INTERNAL SCHEMATIC DIAGRAM



#### ABSOLUTE MAXIMUM RATINGS

Symbol	Parameter	Value		Unit
		BD135	BD139	
$V_{CBO}$	Collector-Base Voltage ( $I_E = 0$ )	45	80	V
$V_{CEO}$	Collector-Emitter Voltage ( $I_B = 0$ )	45	80	V
$V_{EBO}$	Emitter-Base Voltage ( $I_C = 0$ )	5		V
$I_C$	Collector Current	1.5		A
$I_{CM}$	Collector Peak Current	3		A
$I_B$	Base Current	0.5		A
$P_{tot}$	Total Dissipation at $T_o \leq 25^\circ\text{C}$	12.5		W
$P_{tot}$	Total Dissipation at $T_{amb} \leq 25^\circ\text{C}$	1.25		W
$T_{stg}$	Storage Temperature	-65 to 150		$^\circ\text{C}$
$T_j$	Max. Operating Junction Temperature	150		$^\circ\text{C}$

## THERMAL DATA

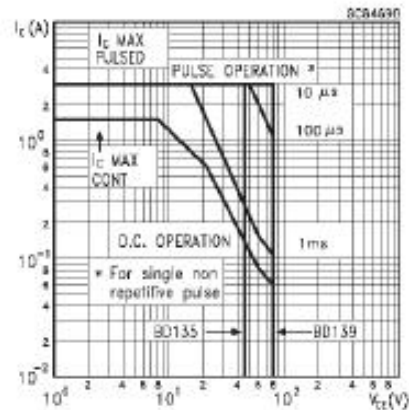
$R_{th(j-case)}$	Thermal Resistance Junction-case	Max	10	$^{\circ}\text{C}/\text{W}$
------------------	----------------------------------	-----	----	-----------------------------

ELECTRICAL CHARACTERISTICS ( $T_{case} = 25^{\circ}\text{C}$  unless otherwise specified)

Symbol	Parameter	Test Conditions	Min.	Typ.	Max.	Unit
$I_{CBO}$	Collector Cut-off Current ( $I_E = 0$ )	$V_{CB} = 30\text{ V}$ $V_{CB} = 30\text{ V}$ $T_C = 125^{\circ}\text{C}$			0.1 10	$\mu\text{A}$ $\mu\text{A}$
$I_{EBO}$	Emitter Cut-off Current ( $I_C = 0$ )	$V_{EB} = 5\text{ V}$			10	$\mu\text{A}$
$V_{CE(sus)}^*$	Collector-Emitter Sustaining Voltage	$I_C = 30\text{ mA}$ for BD135 for BD139	45 80			V V
$V_{CE(sat)}^*$	Collector-Emitter Saturation Voltage	$I_C = 0.5\text{ A}$ $I_B = 0.05\text{ A}$			0.5	V
$V_{BE}^*$	Base-Emitter Voltage	$I_C = 0.5\text{ A}$ $V_{CE} = 2\text{ V}$			1	V
$h_{FE}^*$	DC Current Gain	$I_C = 5\text{ mA}$ $V_{CE} = 2\text{ V}$ $I_C = 0.5\text{ A}$ $V_{CE} = 2\text{ V}$ $I_C = 150\text{ mA}$ $V_{CE} = 2\text{ V}$	25 25 40		250	
$h_{FE}$	$h_{FE}$ Groups	$I_C = 150\text{ mA}$ $V_{CE} = 2\text{ V}$ for BD139 group 10	63		160	

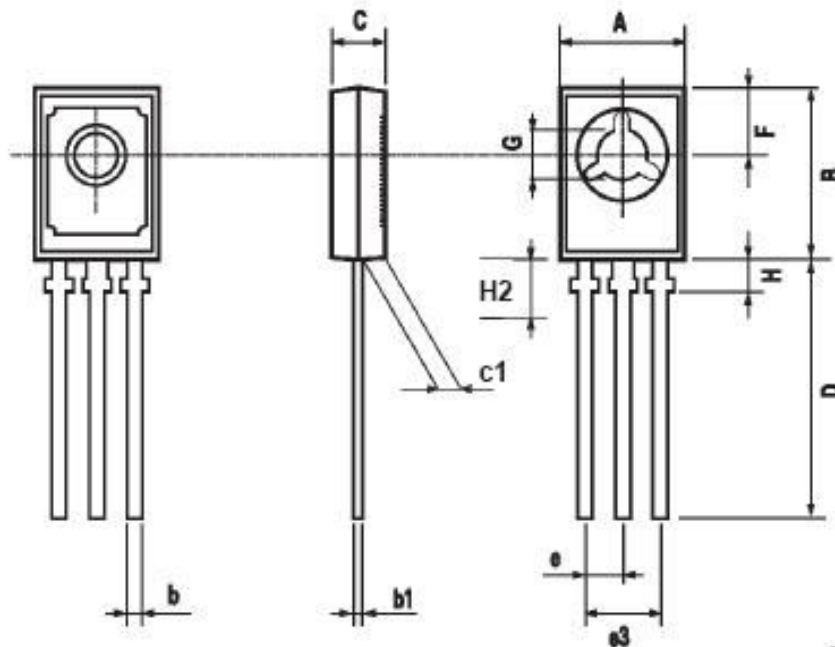
\* Pulsed: Pulse duration = 300  $\mu\text{s}$ , duty cycle 1.5 %

## Safe Operating Area



## SOT-32 (TO-126) MECHANICAL DATA

DIM.	mm			inch		
	MIN.	TYP.	MAX.	MIN.	TYP.	MAX.
A	7.4		7.8	0.291		0.307
B	10.5		10.8	0.413		0.445
b	0.7		0.9	0.028		0.035
b1	0.49		0.75	0.019		0.030
C	2.4		2.7	0.040		0.106
c1	1.0		1.3	0.039		0.050
D	15.4		16.0	0.606		0.629
e		2.2			0.087	
e3	4.15		4.65	0.163		0.183
F		3.8			0.150	
G	3		3.2	0.118		0.126
H			2.54			0.100



0016114